

Three-body Fermi-liquid corrections for Andreev transport through quantum dots

Akira Oguri,^{1,2} Masashi Hashimoto,¹ and Yoshimichi Teratani^{1,2}

¹*Department of Physics, Osaka City University, Sumiyoshi-ku, Osaka, 558-8585, Japan*
²*NITEP, Osaka Metropolitan University, Sumiyoshi-ku, Osaka, 558-8585, Japan*

(Dated: February 16, 2026)

We study crossed Andreev reflection occurring in quantum dots connected to one superconducting lead and two normal leads at low temperatures T . Specifically, we derive an exact formula for the conductance up to order T^2 in the large superconducting gap limit, which is expressed in terms of the transmission probabilities of Cooper pairs and interacting Bogoliubov quasiparticles. Our formulation is based on the latest version of Fermi-liquid theory for the Anderson impurity model, which has clarified the quasiparticle energy shifts of order ω^2 and T^2 —that is, corrections of the same order as those arising from the finite lifetime of quasiparticles—can be exactly taken into account through three-body correlations of impurity electrons. We also demonstrate how the three-body contributions evolve and affect the Cooper-pair tunneling as the Andreev level moves away from the Fermi level, using the numerical renormalization group approach. The results demonstrate that the Cooper-pair contribution to the T^2 term of the nonlocal conductance becomes comparable to the Bogoliubov-quasiparticle contribution in the parameter region where superconducting proximity effects dominate over the Kondo effect.

I. INTRODUCTION

Andreev reflection in quantum dots (QD) connected to multiterminal networks consisting of normal (N) and superconducting (SC) leads is an active field of current research [1–4]. In particular, crossed Andreev reflection (CAR) is one of the most interesting processes arising from Cooper-pair tunneling in which an incident electron entering from a normal lead forms a Cooper pair with another electron from a different normal lead to tunnel into the superconducting leads, leaving behind a hole in the normal lead where the second electron came from. The CAR is also related, via time-reversal symmetry, to Cooper-pair splitting processes, in which a Cooper pair emitted from the superconducting lead splits into two entangled electrons that propagate into different normal leads [5–17].

Moreover, the Coulomb interaction between electrons in quantum dots induces an interesting crossover between the Kondo singlet and the Cooper-pair singlet [18–48]. Contributions from CAR can be detected through the nonlocal conductance, measured via the current flowing from the quantum dot to the normal drain electrode under a bias voltage applied to the source electrode. However, the nonlocal conductance also contains contributions from direct single-electron tunneling, in which an incident electron from the source electrode is transmitted directly to the drain electrode through the quantum dot. In order to extract the CAR contributions, it is therefore essential to clarify the conditions under which Cooper-pair tunneling dominates the nonlocal conductance, taking into account competing effects arising from electron correlations and quantum-interference effects [49, 50].

The low-energy properties of Kondo systems in quantum dots have been extensively studied through highly sensitive transport measurements [51–64]. Transport properties have also been theoretically investigated for electrical currents [65–70], shot noise [71–75], and ther-

mal conductivity [76, 77]. The underlying physics of low-lying energy states that exhibit universal behavior can be explained in terms of Fermi-liquid theory [78–82]. In particular, recent developments in Fermi-liquid theory have revealed the fact that three-body correlations between impurity electrons play an essential role in the next-to-leading-order terms of the transport coefficients at finite frequencies ω , temperatures T , and bias voltages eV , when particle-hole symmetry, time-reversal symmetry, or both are broken [83–99]. This follows from rigorous proofs showing that the quasiparticle energy shifts of order ω^2 , T^2 , and $(eV)^2$ —that is, corrections of the same order as those arising from the finite lifetime of quasiparticles—can be expressed in terms of three-body correlations of impurity electrons.

The purpose of this paper is to present a comprehensive analysis of Andreev transport through a strongly correlated quantum state at finite temperatures $T \neq 0$, with explicit inclusion of three-body correlations. To this

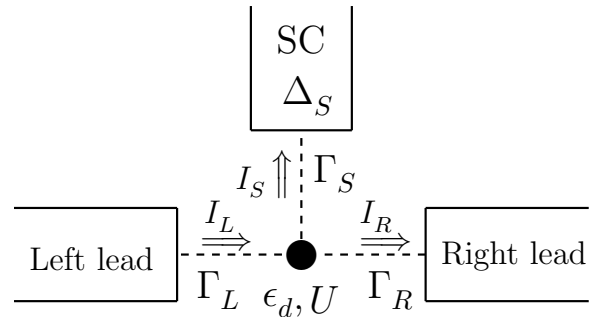


FIG. 1. Anderson impurity (●) coupled to one superconducting (SC) lead and two normal leads on the left and right. Δ_S is the SC gap, and ϵ_d and U are the level position and Coulomb interaction of the impurity electrons. Γ_L , Γ_R , and Γ_S represent the tunneling couplings between the impurity site and the left (L), right (R), and SC leads, respectively.

end, we focus on a quantum-dot system connected to two normal leads and one superconducting lead, which is described by the Anderson impurity model illustrated in Fig. 1. We derive a formula for the linear conductance up to order T^2 based on the latest version of Fermi-liquid theory in the large superconducting-gap limit and show that the conductance is determined by the transmission probabilities of Cooper pairs, $\mathcal{T}_{\text{CP}}(T)$, and Bogoliubov quasiparticles, $\mathcal{T}_{\text{BG}}(T)$. Their low-temperature expansion are given by

$$\mathcal{T}_{\text{CP}}(T) = \frac{1}{4} \sin^2 \theta \sin^2(\delta_{\uparrow} + \delta_{\downarrow}) + c_T^{\text{CP}} (\pi T)^2 + O(T^4),$$

$$\mathcal{T}_{\text{BG}}(T) = \frac{1}{2} \sum_{\sigma=\uparrow,\downarrow} \sin^2 \delta_{\sigma} - c_T^{\text{BG}} (\pi T)^2 + O(T^4).$$

The leading-order terms on the right-hand side correspond to the ground-state values, where δ_{σ} denotes the phase shift of interacting Bogoliubov quasiparticles and θ is the Bogoliubov rotation angle [49]. The coefficients c_T^{CP} and c_T^{BG} of the T^2 terms are expressed in terms of the linear susceptibilities $\chi_{\sigma_1\sigma_2}$ and the three-body correlation functions $\chi_{\sigma_1\sigma_2\sigma_3}^{[3]}$ of the Bogoliubov quasiparticles. We show that the Cooper-pair contribution c_T^{CP} can be expressed in the following form:

$$c_T^{\text{CP}} = -\frac{\pi^2}{3} \frac{1}{4} \sin^2 \theta \left[-\cos(2\delta_{\uparrow} + 2\delta_{\downarrow}) (\chi_{\uparrow\uparrow} - \chi_{\downarrow\downarrow})^2 + \frac{\sin(2\delta_{\uparrow} + 2\delta_{\downarrow})}{2\pi} (\chi_{\uparrow\uparrow\uparrow}^{[3]} + \chi_{\uparrow\uparrow\downarrow}^{[3]} + \chi_{\downarrow\downarrow\downarrow}^{[3]} + \chi_{\downarrow\downarrow\uparrow}^{[3]}) \right].$$

By contrast, the Bogoliubov-quasiparticle contribution c_T^{BG} is identical to that for normal electrons tunneling through an N/QD/N junction, studied previously [85–89]. In particular, at zero magnetic field, the Cooper-pair contribution c_T^{CP} is determined solely by the three-body correlations.

We also calculate these coefficients, together with the three-body correlation functions, using Wilson's numerical renormalization group (NRG) at zero magnetic field. The results show that the Cooper-pair contribution c_T^{CP} becomes comparable to c_T^{BG} in the parameter region where superconducting pair correlation is enhanced in the quantum dot, whereas c_T^{BG} dominates the T^2 term in the Kondo regime. These coefficients c_T^{BG} and c_T^{CP} can also be experimentally extracted by measuring the T^2 terms of both the nonlocal g_{RL} and local g_{LL} conductances.

This paper is organized as follows. In Sec. II, we introduce an Anderson impurity model for quantum dots connected to normal and superconducting leads, and reformulate the Hamiltonian and correlation functions in terms of interacting Bogoliubov quasiparticles. Section III is devoted to the Fermi-liquid description of interacting Bogoliubov quasiparticles, in which three-body correlations play an essential role. An exact conductance formula valid up to order T^2 is also presented, while detailed derivations are deferred to the final part of this

paper. In Sec. IV, we present NRG results that demonstrate how the three-body corrections affect the next-to-leading-order terms in crossed Andreev reflection. In Sec. V, we provide the derivation of the conductance formula to order T^2 , leaving the precise analysis of the superconducting collision integrals required for the complete proof to the Appendix. A summary and discussion are given in Sec. VI.

II. FERMI-LIQUID DESCRIPTION FOR BOGOLIUBOV QUASIPARTICLES

In this section, we begin with an Anderson impurity model describing a single quantum dot (QD) connected to one superconducting (SC) lead and two normal (N) leads, and then transform it into a system of interacting Bogoliubov quasiparticles, the total number of which is conserved. We also introduce three-body correlation functions of the Bogoliubov quasiparticles, which determine the next-to-leading-order terms of the transport coefficients in the low-energy Fermi-liquid regime.

A. Anderson impurity model for the CAR

We consider the Anderson impurity model for the quantum dot system as shown in Fig. 1:

$$H = H_d^0 + H_d^U + H_N + H_{\text{TN}} + H_S + H_{\text{TS}}, \quad (2.1)$$

$$H_d^0 = \xi_d (n_d - 1) - b (n_{d\uparrow} - n_{d\downarrow}), \quad (2.2)$$

$$H_d^U = \frac{U}{2} (n_d - 1)^2, \quad (2.3)$$

$$H_N = \sum_{j=L,R} \sum_{\sigma} \int_{-D}^D d\epsilon \epsilon c_{\epsilon j\sigma}^{\dagger} c_{\epsilon j\sigma}, \quad (2.4)$$

$$H_{\text{TN}} = - \sum_{j=L,R} v_j \sum_{\sigma} \int_{-D}^D d\epsilon \sqrt{\rho_c} (c_{\epsilon j\sigma}^{\dagger} d_{\sigma} + \text{H.c.}), \quad (2.5)$$

$$H_{\text{TS}} = -v_S \sum_{\sigma} \int_{-D_S}^{D_S} d\epsilon \sqrt{\rho_S} (s_{\epsilon\sigma}^{\dagger} d_{\sigma} + \text{H.c.}), \quad (2.6)$$

$$H_S = \sum_{\sigma} \int_{-D_S}^{D_S} d\epsilon \epsilon s_{\epsilon\sigma}^{\dagger} s_{\epsilon\sigma} + \int_{-D_S}^{D_S} d\epsilon (\Delta_S s_{\epsilon\uparrow}^{\dagger} s_{\epsilon\downarrow}^{\dagger} + \text{H.c.}). \quad (2.7)$$

Here, H_d^0 and H_d^U , correspond to the Hamiltonian for electrons in the QD. The parameter $\xi_d \equiv \epsilon_d + U/2$ is defined in terms of the discrete energy level ϵ_d and the Coulomb interaction U . The Zeeman energy due to a magnetic field B applied to the QD is given by $b \equiv \mu_B B$, with μ_B the Bohr magneton. The operator d_{σ}^{\dagger} creates an electron with spin σ ($=\uparrow, \downarrow$), and $n_d \equiv n_{d\uparrow} + n_{d\downarrow}$ is the total number operator, with $n_{d\sigma} \equiv d_{\sigma}^{\dagger} d_{\sigma}$.

H_N describes the conduction electrons in the normal leads, for which the density of states is assumed to be a constant $\rho_c = 1/(2D)$, with D the half-width of the

bands. The Fermi level is set at the center of the conduction bands, $E_F \equiv 0$. The operator $c_{\epsilon j \sigma}^\dagger$ creates a conduction electron with spin σ and energy ϵ in the left ($j = L$) or right ($j = R$) lead. The operators satisfy the anti-commutation relation, $\{c_{\epsilon j \sigma}, c_{\epsilon' j' \sigma'}^\dagger\} = \delta_{jj'} \delta_{\sigma\sigma'} \delta(\epsilon - \epsilon')$, which is normalized by the Dirac delta function. H_{TN} describes the tunnel coupling between the QD and the normal leads. The level broadening of the discrete energy level in the QD is given by $\Gamma_N \equiv \Gamma_L + \Gamma_R$, with $\Gamma_j \equiv \pi \rho_c v_j^2$.

H_S and H_{TS} describe the superconducting lead and its tunnel coupling to the QD, characterized by an s -wave superconducting gap $\Delta_S \equiv |\Delta_S| e^{i\phi_S}$. The operator $s_{\epsilon \sigma}^\dagger$ creates an electron with spin σ and energy ϵ in the SC lead, with D_S the half-band width and $\rho_S = 1/(2D_S)$. The coupling strength between the QD and the SC lead is given by $\Gamma_S \equiv \pi \rho_S v_S^2$, and it serves as one of the key parameters characterizing the superconducting proximity effect in this system.

The current operators, $\hat{I}_{R,\sigma}$, flowing from the QD to the right normal lead, and $\hat{I}_{L,\sigma}$, flowing from the left normal lead to the QD, are given by

$$\hat{I}_{R,\sigma} = i e v_R \int_{-D}^D d\epsilon \sqrt{\rho_c} (c_{\epsilon,R,\sigma}^\dagger d_\sigma - d_\sigma^\dagger c_{\epsilon,R,\sigma}), \quad (2.8)$$

$$\hat{I}_{L,\sigma} = -i e v_L \int_{-D}^D d\epsilon \sqrt{\rho_c} (c_{\epsilon,L,\sigma}^\dagger d_\sigma - d_\sigma^\dagger c_{\epsilon,L,\sigma}), \quad (2.9)$$

for each spin component σ . We consider the situation in which a bias voltage V_j is applied to the normal leads ($j = L, R$) via their chemical potentials, such that $\mu_j \equiv eV_j$ and $V \equiv V_L - V_R$. In addition, the chemical potential μ_S of the SC lead is set at the center of the conduction band, i.e., $\mu_S \equiv 0$.

B. Effective Hamiltonian for large-gap limit

In this paper, we investigate transport properties at finite temperatures much lower than the superconducting energy gap. Specifically, we consider the large-gap limit, $|\Delta_S| \rightarrow \infty$, in which the influence of Cooper-pair tunneling on the QD and normal leads can be described by an effective Hamiltonian \mathcal{H}_{eff} [24, 30]:

$$\mathcal{H}_{\text{eff}} \equiv \Delta_d d_\uparrow^\dagger d_\downarrow^\dagger + \Delta_d^* d_\downarrow d_\uparrow + H_{\text{dot}} + H_N + H_{\text{TN}}, \quad (2.10)$$

$$\Delta_d \equiv \Gamma_S e^{i\phi_S}, \quad H_{\text{dot}} \equiv H_d^0 + H_d^U. \quad (2.11)$$

Here, the SC part of the Hamiltonian, $H_S + H_{\text{TS}}$, has been replaced by the local pair potential Δ_d penetrating into the impurity site. In the following, we will choose the gauge of the electron operators such that it absorbs the Josephson phase of Δ_d , i.e., $\phi_S = 0$.

This effective Hamiltonian possesses a global U(1) symmetry in the Nambu pseudo-spin space, which becomes explicit upon performing the Bogoliubov transfor-

mation:

$$\begin{pmatrix} \gamma_{d\uparrow} \\ \gamma_{d\downarrow}^\dagger \end{pmatrix} = \mathcal{U}^\dagger \begin{pmatrix} d_\uparrow \\ d_\downarrow^\dagger \end{pmatrix}, \quad \begin{pmatrix} \gamma_{\epsilon,j,\uparrow} \\ -\gamma_{-\epsilon,j,\downarrow}^\dagger \end{pmatrix} = \mathcal{U}^\dagger \begin{pmatrix} c_{\epsilon,j,\uparrow} \\ -c_{-\epsilon,j,\downarrow}^\dagger \end{pmatrix}. \quad (2.12)$$

The matrix \mathcal{U} can be expressed in the following form:

$$\mathcal{U} \equiv \begin{pmatrix} \cos \frac{\theta}{2} & -\sin \frac{\theta}{2} \\ \sin \frac{\theta}{2} & \cos \frac{\theta}{2} \end{pmatrix}, \quad (2.13)$$

$$\cos \frac{\theta}{2} = \sqrt{\frac{1}{2} \left(1 + \frac{\xi_d}{E_A} \right)}, \quad \sin \frac{\theta}{2} = \sqrt{\frac{1}{2} \left(1 - \frac{\xi_d}{E_A} \right)}.$$

Here, $E_A \equiv \sqrt{\xi_d^2 + \Gamma_S^2}$, $\sin \theta = \frac{\Gamma_S}{E_A}$, and $\cos \theta = \frac{\xi_d}{E_A}$. This transformation maps the effective Hamiltonian \mathcal{H}_{eff} onto a system of interacting Bogoliubov quasiparticles, which is described by a standard Anderson impurity model with a conserved charge:

$$\begin{aligned} \mathcal{H}_{\text{eff}} = & E_A \left(\sum_\sigma \gamma_{d\sigma}^\dagger \gamma_{d\sigma} - 1 \right) - b \left(\gamma_{d\uparrow}^\dagger \gamma_{d\uparrow} - \gamma_{d\downarrow}^\dagger \gamma_{d\downarrow} \right) \\ & + \frac{U}{2} \left(\sum_\sigma \gamma_{d\sigma}^\dagger \gamma_{d\sigma} - 1 \right)^2 + \sum_{j=L,R} \sum_\sigma \int_{-D}^D d\epsilon \epsilon \gamma_{\epsilon,j,\sigma}^\dagger \gamma_{\epsilon,j,\sigma} \\ & + \sum_{j=L,R} v_j \sum_\sigma \int_{-D}^D d\epsilon \sqrt{\rho_c} \left(\gamma_{\epsilon,j,\sigma}^\dagger \gamma_{d\sigma} + \text{H.c.} \right). \end{aligned} \quad (2.14)$$

This representation explicitly shows that the total number of Bogoliubov quasiparticles \mathcal{N}_γ is conserved, reflecting the global U(1) symmetry along the principal axis of the Nambu pseudo-spin space:

$$\mathcal{N}_\gamma \equiv \sum_\sigma \gamma_{d\sigma}^\dagger \gamma_{d\sigma} + \sum_{j=L,R} \sum_\sigma \int_{-D}^D d\epsilon \gamma_{\epsilon,j,\sigma}^\dagger \gamma_{\epsilon,j,\sigma}. \quad (2.15)$$

In particular, the occupation number $q_{d\sigma}$ of Bogoliubov quasiparticles in the QD plays a central role in the ground-state properties:

$$q_{d\sigma} \equiv \gamma_{d\sigma}^\dagger \gamma_{d\sigma}, \quad q_d \equiv q_{d\uparrow} + q_{d\downarrow}. \quad (2.16)$$

Figure 2 illustrates the parameter space of \mathcal{H}_{eff} at zero magnetic field, $b = 0$. The polar angle $\theta = \cot^{-1}(\xi_d/\Gamma_S)$ corresponds to the Bogoliubov rotation angle. In the atomic limit $\Gamma_N \rightarrow 0$, the impurity level is occupied by a single Bogoliubov quasiparticle, $\langle q_d \rangle = 1.0$, inside the semicircle $E_A < U/2$, whereas it becomes empty, $\langle q_d \rangle = 0.0$, outside the semicircle $E_A > U/2$. As the coupling Γ_N is switched on, conduction electrons from the normal leads screen the local moment, and the Kondo singlet becomes the ground state inside the semicircle. Valence-fluctuation behavior of the Bogoliubov quasiparticles also appears near the boundary $E_A \simeq U/2$. In particular, it manifests itself as a crossover between the Kondo singlet and the superconductivity-induced singlet at $\theta \simeq \pi/2$. Correspondingly, crossed Andreev scattering is enhanced at $T = 0$ in the angular range $\pi/4 \lesssim \theta \lesssim 3\pi/4$ in the vicinity just outside the semicircle for $E_A \gtrsim U/2$ [49].

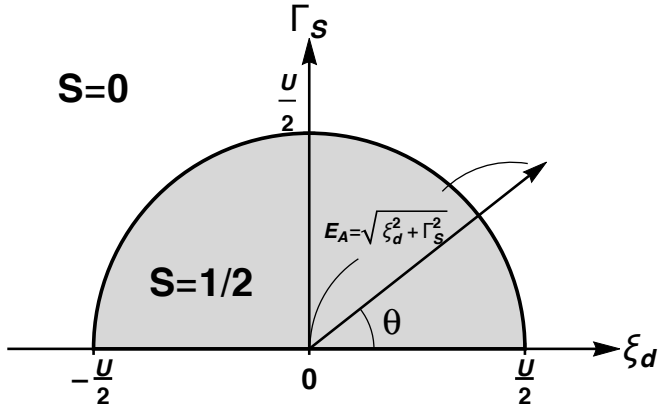


FIG. 2. Parameter space of \mathcal{H}_{eff} at zero magnetic field $b = 0$, defined in Eq. (2.10). Here, $\theta \equiv \cot^{-1}(\xi_d/\Gamma_S)$ is the Bogoliubov rotation angle, with $\xi_d \equiv \epsilon_d + U/2$. The semicircle corresponds to the line along which the energy of the Andreev level, $E_A \equiv \sqrt{\xi_d^2 + \Gamma_S^2}$, coincides with $U/2$. In the atomic limit $\Gamma_N = 0$, the ground state is a magnetic spin doublet ($S = 1/2$) inside the semicircle, which is eventually screened by conduction electrons to form the Kondo singlet when the tunnel coupling Γ_N is switched on, whereas outside the semicircle the ground state is a spin singlet ($S = 0$) due to Cooper pairing.

C. Phase shift of interacting Bogoliubov quasiparticles

We use the following retarded Green's function to describe the transport properties of the QD connected to the SC lead:

$$\mathbf{G}_{dd}^r(\omega) \equiv -i \int_0^\infty dt e^{i(\omega+i0^+)t} \times \begin{pmatrix} \langle \{d_\uparrow(t), d_\uparrow^\dagger\} \rangle_V & \langle \{d_\uparrow(t), d_\downarrow\} \rangle_V \\ \langle \{d_\downarrow^\dagger(t), d_\uparrow^\dagger\} \rangle_V & \langle \{d_\downarrow^\dagger(t), d_\downarrow\} \rangle_V \end{pmatrix}. \quad (2.17)$$

Here, the average $\langle \dots \rangle_V$ is defined with respect to the nonequilibrium steady state, constructed at finite bias voltage eV and temperature T , using the Keldysh formalism [65, 100, 101]. This matrix, \mathbf{G}_{dd}^r , can be diagonalized by the Bogoliubov transformation:

$$\tilde{\mathbf{G}}^r(\omega) \equiv \mathbf{U}^\dagger \mathbf{G}_{dd}^r(\omega) \mathbf{U}$$

$$= \begin{pmatrix} \tilde{G}_1^r(\omega) & 0 \\ 0 & \tilde{G}_2^r(\omega) \end{pmatrix} = \begin{pmatrix} G_{\gamma,\uparrow}^r(\omega) & 0 \\ 0 & -G_{\gamma,\downarrow}^a(-\omega) \end{pmatrix}. \quad (2.18)$$

Here, $G_{\gamma,\sigma}^r$ and $G_{\gamma,\sigma}^a$ correspond to the retarded and advanced Green's functions, respectively, for Bogoliubov

quasiparticles in the QD:

$$\begin{aligned} G_{\gamma,\sigma}^r(\omega) &\equiv -i \int_0^\infty dt e^{i(\omega+i0^+)t} \langle \{ \gamma_{d\sigma}(t), \gamma_{d\sigma}^\dagger \} \rangle_V \\ &= \frac{1}{\omega - E_{A,\sigma} + i\Gamma_N - \Sigma_{\gamma,\sigma}^r(\omega)}, \end{aligned} \quad (2.19)$$

and $G_{\gamma,\sigma}^a(\omega) = \{G_{\gamma,\sigma}^r(\omega)\}^*$. Here, $E_{A,\uparrow} \equiv E_A - b$ and $E_{A,\downarrow} \equiv E_A + b$, and $\Sigma_{\gamma,\sigma}^r(\omega)$ represents the self-energy correction arising from the interaction Hamiltonian H_d^U defined in Eq. (2.3), which can alternatively be expressed in the form $H_d^U = \frac{U}{2}(q_d - 1)^2$. In the noninteracting limit $H_d^U \rightarrow 0$, Eq. (2.19) describes an Andreev resonance level located at $\omega = E_{A,\sigma}$ with a width Γ_N .

The phase shift δ_σ of the Bogoliubov quasiparticles, defined by $G_{\gamma,\sigma}^r(0) = -|G_{\gamma,\sigma}(0)|e^{i\delta_\sigma}$ at $T = eV = 0$, plays a central role in the ground-state properties. In particular, the Friedel sum rule holds for the average occupation number $\langle q_{d\sigma} \rangle$ of the Bogoliubov quasiparticles in the QD, namely,

$$\langle q_{d\sigma} \rangle \xrightarrow{T \rightarrow 0} \frac{\delta_\sigma}{\pi}. \quad (2.20)$$

Here, $\langle \mathcal{O} \rangle = \text{Tr}[e^{-\beta \mathcal{H}_{\text{eff}}} \mathcal{O}]/\text{Tr} e^{-\beta \mathcal{H}_{\text{eff}}}$ denotes the equilibrium average, with $\beta \equiv 1/T$. The phase shift reaches $\delta_\sigma = \pi/2$ at $E_A = 0$ and decreases as E_A increases along the radial direction in the $\xi_d - \Gamma_S$ plane shown in Fig. 2, while it remains independent of the polar angle θ .

The ground-state properties of electrons, such as the occupation number $\langle n_d \rangle$ and the superconducting pair correlation function $\langle d_\uparrow^\dagger d_\downarrow^\dagger + d_\downarrow d_\uparrow \rangle$, can be derived from $\langle q_d \rangle$ as follows:

$$\langle n_d \rangle - 1 = (\langle q_d \rangle - 1) \cos \theta, \quad (2.21)$$

$$\langle d_\uparrow^\dagger d_\downarrow^\dagger + d_\downarrow d_\uparrow \rangle = (\langle q_d \rangle - 1) \sin \theta. \quad (2.22)$$

These two averages correspond, respectively, to the projections of a vector of magnitude $\langle q_d \rangle - 1$, oriented along the principal axis, onto the z and x axes of the Nambu pseudo-spin space. Similarly, the local magnetization m_d , which can be induced in the QD at finite magnetic fields, can be expressed as

$$m_d \equiv \langle n_{d\uparrow} \rangle - \langle n_{d\downarrow} \rangle = \langle q_{d\uparrow} \rangle - \langle q_{d\downarrow} \rangle. \quad (2.23)$$

D. Susceptibilities and Three-body correlations

The low-energy properties of the effective Hamiltonian \mathcal{H}_{eff} can be described within the framework of Fermi-liquid theory using a set of essential parameters: the occupation numbers $\langle q_{d\sigma} \rangle$, the linear susceptibilities $\chi_{\sigma_1\sigma_2}$, and the three-body correlation functions $\chi_{\sigma_1\sigma_2\sigma_3}^{[3]}$, defined

by

$$\langle q_{d\sigma} \rangle = \frac{\partial \Omega_{\text{eff}}}{\partial E_{A,\sigma}}, \quad (2.24)$$

$$\chi_{\sigma_1\sigma_2} \equiv -\frac{\partial \Omega_{\text{eff}}}{\partial E_{A,\sigma_1} \partial E_{A,\sigma_2}} = \int_0^\beta d\tau \langle \delta q_{d\sigma_1}(\tau) \delta q_{d\sigma_2} \rangle, \quad (2.25)$$

$$\begin{aligned} \chi_{\sigma_1\sigma_2\sigma_3}^{[3]} &\equiv -\frac{\partial^3 \Omega_{\text{eff}}}{\partial E_{A,\sigma_1} \partial E_{A,\sigma_2} \partial E_{A,\sigma_3}} \\ &= -\int_0^\beta d\tau \int_0^\beta d\tau' \langle T_\tau \delta q_{d\sigma_1}(\tau) \delta q_{d\sigma_2}(\tau') \delta q_{d\sigma_3} \rangle. \end{aligned} \quad (2.26)$$

Here, $\Omega_{\text{eff}} \equiv -\frac{1}{\beta} \ln [\text{Tr} e^{-\beta \mathcal{H}_{\text{eff}}}]$ is the free energy defined with respect to \mathcal{H}_{eff} . The operator $\delta q_{d\sigma}(\tau) \equiv e^{\tau \mathcal{H}_{\text{eff}}} \delta q_{d\sigma} e^{-\tau \mathcal{H}_{\text{eff}}}$ represents the fluctuation $\delta q_{d\sigma} \equiv q_{d\sigma} - \langle q_{d\sigma} \rangle$ of local Bogoliubov quasiparticles, and T_τ is the imaginary-time ordering operator. Specifically, the ground-state values of these correlation functions, namely, $\langle q_{d\sigma} \rangle$, $\chi_{\sigma_1\sigma_2}$, and $\chi_{\sigma_1\sigma_2\sigma_3}^{[3]}$ defined at $T = 0$, completely determine the transport properties in the Fermi-liquid regime up to the next-to-leading order.

One of the typical Fermi-liquid corrections arising from many-body scattering appears in the T -linear specific heat of impurity electrons, $\mathcal{C}_{\text{imp}}^{\text{heat}}$, which can be expressed in terms of the diagonal components of the linear susceptibility $\chi_{\sigma\sigma}$:

$$\mathcal{C}_{\text{imp}}^{\text{heat}} = \gamma_{\text{imp}} T, \quad \gamma_{\text{imp}} \equiv \frac{\pi^2}{3} \sum_{\sigma} \chi_{\sigma\sigma}. \quad (2.27)$$

This formula was derived by Yamada and Yosida using the Ward identity [79, 81, 82]. In particular, at zero magnetic field $b = 0$, where the two diagonal components coincide, i.e., $\chi_{\uparrow\uparrow} = \chi_{\downarrow\downarrow}$, the T -linear specific heat can be written as $\mathcal{C}_{\text{imp}}^{\text{heat}} = \frac{\pi^2}{6} \frac{T}{T^*}$, where the Fermi-liquid energy scale T^* is defined by

$$T^* \equiv \frac{1}{4\chi_{\uparrow\uparrow}}. \quad (2.28)$$

Correspondingly, the off-diagonal susceptibility $\chi_{\uparrow\downarrow}$ can be naturally scaled by T^* , which leads to the definition of the Wilson ratio R :

$$R - 1 \equiv -\frac{\chi_{\uparrow\downarrow}}{\chi_{\uparrow\uparrow}} = -4T^* \chi_{\uparrow\downarrow}. \quad (2.29)$$

The three-body correlations $\chi_{\sigma_1\sigma_2\sigma_3}^{[3]}$ arise when the particle-hole symmetry, the time-reversal symmetry or both are broken, and they contribute to next-to-leading-order transport properties, such as the T^2 and $(eV)^2$ terms in the conductance. Physically, the three-body correlations give rise to energy shifts of order ω^2 , T^2 , and $(eV)^2$ in the low-lying excitations, corresponding to corrections of the same order as those arising from the finite lifetime of quasiparticles.

III. LINEAR RESPONSE THEORY FOR CAR

In this section, we show how the contributions of crossed Andreev reflection to the nonlocal conductance of the multi-terminal network can be described within the framework of the Fermi-liquid theory for interacting Bogoliubov quasiparticles. Specifically, we consider the linear-response current $I_j \equiv \sum_{\sigma} \langle \hat{I}_{j,\sigma} \rangle_V$ for $j = L, R$, induced by small bias voltages V_L and V_R applied to the left and right leads, respectively:

$$I_R = g_{RL} V_L - g_{RR} V_R, \quad (3.1)$$

$$I_L = -g_{LR} V_R + g_{LL} V_L, \quad (3.2)$$

where the current directions are specified as illustrated in Fig. 1.

A. General formula for T^2 conductance

Here we highlight one of the central results of this work, leaving the derivations to Sec. V. The low-temperature expansion of the linear conductance $g_{jj'} = \partial I_j / \partial V_{j'}$ can be calculated exactly up to terms of order T^2 :

$$g_{RL} = g_{LR} = \frac{2e^2}{h} \frac{4\Gamma_R \Gamma_L}{\Gamma_N^2} \left[\mathcal{T}_{\text{BG}}(T) - 2\mathcal{T}_{\text{CP}}(T) \right], \quad (3.3)$$

$$g_{RR} = \frac{2e^2}{h} \left[\frac{4\Gamma_R \Gamma_L}{\Gamma_N^2} \mathcal{T}_{\text{BG}}(T) + \frac{4\Gamma_R^2}{\Gamma_N^2} 2\mathcal{T}_{\text{CP}}(T) \right], \quad (3.4)$$

$$g_{LL} = \frac{2e^2}{h} \left[\frac{4\Gamma_R \Gamma_L}{\Gamma_N^2} \mathcal{T}_{\text{BG}}(T) + \frac{4\Gamma_L^2}{\Gamma_N^2} 2\mathcal{T}_{\text{CP}}(T) \right]. \quad (3.5)$$

Specifically, the transmission probability for Bogoliubov quasiparticles, $\mathcal{T}_{\text{BG}}(T)$, and that for Cooper pairs, $\mathcal{T}_{\text{CP}}(T)$, can be expanded up to order T^2 as follows:

$$\mathcal{T}_{\text{BG}}(T) = \frac{1}{2} \sum_{\sigma} \sin^2 \delta_{\sigma} - c_T^{\text{BG}} (\pi T)^2 + \dots, \quad (3.6)$$

$$\mathcal{T}_{\text{CP}}(T) = \frac{1}{4} \sin^2 \theta \sin^2(\delta_{\uparrow} + \delta_{\downarrow}) + c_T^{\text{CP}} (\pi T)^2 + \dots \quad (3.7)$$

At $T = 0$, these transmission probabilities are determined by the phase shifts δ_{σ} and the Bogoliubov angle θ , and are bounded as $0 \leq \mathcal{T}_{\text{BG}}(0) \leq 1$ and $0 \leq \mathcal{T}_{\text{CP}}(0) \leq 1/4$. In contrast, the coefficients c_T^{BG} and c_T^{CP} of the T^2 terms depend also on the susceptibilities $\chi_{\sigma_1\sigma_2}$ and the

three-body correlation functions $\chi_{\sigma_1\sigma_2\sigma_3}^{[3]}$:

$$c_T^{\text{BG}} \equiv \frac{\pi^2}{3} \frac{1}{2} \sum_{\sigma=\uparrow,\downarrow} \left[-\cos 2\delta_\sigma \left(\chi_{\sigma\sigma}^2 + 2\chi_{\uparrow\downarrow}^2 \right) + \frac{\sin 2\delta_\sigma}{2\pi} \left(\chi_{\sigma\sigma\sigma}^{[3]} + \chi_{\sigma\sigma\sigma}^{[3]} \right) \right], \quad (3.8)$$

$$c_T^{\text{CP}} \equiv -\frac{\pi^2}{3} \frac{1}{4} \sin^2 \theta \left[-\cos(2\delta_\uparrow + 2\delta_\downarrow) \left(\chi_{\uparrow\uparrow} - \chi_{\downarrow\downarrow} \right)^2 + \frac{\sin(2\delta_\uparrow + 2\delta_\downarrow)}{2\pi} \left(\chi_{\uparrow\uparrow\uparrow}^{[3]} + \chi_{\uparrow\downarrow\downarrow}^{[3]} + \chi_{\downarrow\downarrow\downarrow}^{[3]} + \chi_{\downarrow\uparrow\uparrow}^{[3]} \right) \right]. \quad (3.9)$$

Here, $\bar{\sigma}$ represents an opposite spin component of σ , i.e., $\bar{\uparrow} = \downarrow$ and $\bar{\downarrow} = \uparrow$. Note that $\mathcal{T}_{\text{BG}}(T)$ and $\mathcal{T}_{\text{CP}}(T)$ depend on the tunneling couplings only through the total hybridization width $\Gamma_N = \Gamma_L + \Gamma_R$. Thus, the L - R tunnel asymmetry, $(\Gamma_L - \Gamma_R)/\Gamma_N$, influences the linear current I_j solely via the prefactors $\Gamma_R\Gamma_L/\Gamma_N^2$, Γ_R^2/Γ_N^2 , and Γ_L^2/Γ_N^2 that appear explicitly in Eqs. (3.3)–(3.5).

The Bogoliubov-quasiparticle contribution, $\mathcal{T}_{\text{BG}}(T)$, does not depend on the angle θ . Its expression, given by Eqs. (3.6) and (3.8), is identical to that of the conductance for normal electrons tunneling through a N/QD/N junction [85–89]. The θ dependence of Cooper-pair contribution, $\mathcal{T}_{\text{CP}}(T)$, is entirely determined by the superconducting coherence factor, $\sin^2 \theta$, namely, both the leading term $\mathcal{T}_{\text{CP}}(0)$ and the coefficient c_T^{CP} are proportional to $\sin^2 \theta$. Therefore, $\mathcal{T}_{\text{BG}}(T)$ and $\mathcal{T}_{\text{CP}}(T)/\sin^2 \theta$ are the functions that vary only along the radial direction in the parameter space shown in Fig. 2. The corresponding Fermi-liquid parameters δ_σ , $\chi_{\sigma_1\sigma_2}$, and $\chi_{\sigma_1\sigma_2\sigma_3}^{[3]}$ are determined by \mathcal{H}_{eff} , given in Eq. (2.14).

The contribution of $\mathcal{T}_{\text{CP}}(T)$ to the nonlocal conductance g_{RL} appears with the opposite sign compared with its contribution to the local conductance g_{LL} , since in the CAR process the electrons from the right (drain) normal lead flow in opposite directions to form a Cooper pair. The current I_S flowing into the SC lead from the QD is determined solely by the Cooper-pair tunneling processes:

$$I_S \equiv I_L - I_R = \frac{4e^2}{h} 4\mathcal{T}_{\text{CP}}(T) V_{\text{SN}}, \quad (3.10)$$

$$V_{\text{SN}} \equiv \frac{\Gamma_L V_L + \Gamma_R V_R}{\Gamma_L + \Gamma_R}, \quad (3.11)$$

where V_{SN} can be regarded as a symmetrized bias voltage between the SC and the normal leads. The corresponding conductance, $g_{\text{SN}} \equiv dI_S/dV_{\text{SN}}$, is equivalent to that investigated previously for an N/QD/SC junction [30], and reaches its maximum value of $4e^2/h$ at $T = 0$ when $4\mathcal{T}_{\text{CP}}(0) = 1$. Similarly, the average of currents I_L and I_R flowing between the QD and the normal leads can be

expressed as:

$$\begin{aligned} \frac{I_L + I_R}{2} &= \frac{2e^2}{h} \frac{4\Gamma_R\Gamma_L}{(\Gamma_L + \Gamma_R)^2} \mathcal{T}_{\text{BG}}(T) (V_L - V_R) \\ &+ \frac{2e^2}{h} \frac{\Gamma_L - \Gamma_R}{\Gamma_L + \Gamma_R} 4\mathcal{T}_{\text{CP}}(T) V_{\text{SN}}. \end{aligned} \quad (3.12)$$

When the tunnel couplings are symmetric, i.e., $\Gamma_L = \Gamma_R$, the Cooper-pair contribution from $\mathcal{T}_{\text{CP}}(T)$ to this average current vanishes, since the currents associated with Andreev scattering of electrons from the left and right normal leads cancel each other out.

B. Conductance at zero magnetic field

Here, we present simplified form of the conductance formulas applicable at zero magnetic field. In the absence of a magnetic field ($b = 0$), time-reversal symmetry reduces the number of independent components of the correlation functions: $\delta_\uparrow = \delta_\downarrow$, $\chi_{\uparrow\uparrow} = \chi_{\downarrow\downarrow}$, $\chi_{\uparrow\uparrow\uparrow}^{[3]} = \chi_{\downarrow\downarrow\downarrow}^{[3]}$, and $\chi_{\uparrow\downarrow\downarrow}^{[3]} = \chi_{\downarrow\uparrow\uparrow}^{[3]}$. Among these, the two independent linear susceptibilities, $\chi_{\uparrow\uparrow}$ and $\chi_{\uparrow\downarrow}$, can be expressed in terms of the Fermi-liquid energy scale T^* and the Wilson ratio R , defined in Eqs. (2.28) and (2.29), respectively. Therefore, the transport probabilities $\mathcal{T}_{\text{BG}}(T)$ and $\mathcal{T}_{\text{CP}}(T)$ simplify and take the following forms:

$$\mathcal{T}_{\text{BG}}(T) \xrightarrow{b \rightarrow 0} \sin^2 \delta - C_T^{\text{BG}} \left(\frac{\pi T}{T^*} \right)^2 + \dots, \quad (3.13)$$

$$\mathcal{T}_{\text{CP}}(T) \xrightarrow{b \rightarrow 0} \frac{1}{4} \sin^2 \theta \sin^2 2\delta + C_T^{\text{CP}} \left(\frac{\pi T}{T^*} \right)^2 + \dots \quad (3.14)$$

Here, the dimensionless coefficients C_T^{BG} and C_T^{CP} of the T^2 terms are defined by

$$C_T^{\text{BG}} = \frac{\pi^2}{48} \left[-\cos 2\delta \left\{ 1 + 2(R - 1)^2 \right\} + \Theta_T^{\text{BG}} \right], \quad (3.15)$$

$$\Theta_T^{\text{BG}} \equiv \frac{\sin 2\delta}{2\pi\chi_{\uparrow\uparrow}^2} \left(\chi_{\uparrow\uparrow\uparrow}^{[3]} + \chi_{\uparrow\downarrow\downarrow}^{[3]} \right), \quad (3.16)$$

and

$$C_T^{\text{CP}} = \frac{\pi^2}{48} \Theta_T^{\text{CP}} \sin^2 \theta, \quad (3.17)$$

$$\Theta_T^{\text{CP}} \equiv -\frac{\sin 4\delta}{4\pi\chi_{\uparrow\uparrow}^2} \left(\chi_{\uparrow\uparrow\uparrow}^{[3]} + \chi_{\uparrow\downarrow\downarrow}^{[3]} \right). \quad (3.18)$$

Note that, at zero magnetic field, the Cooper-pair contribution C_T^{CP} is determined solely by the dimensionless three-body correlation, Θ_T^{CP} , which is proportional to the sum $\chi_{\uparrow\uparrow\uparrow}^{[3]} + \chi_{\uparrow\downarrow\downarrow}^{[3]}$.

1. Three-body correlations for $\mathcal{H}_{\text{eff}} = 0$

In the noninteracting case, $H_d^U = 0$, all off-diagonal components of the linear susceptibilities and three-body

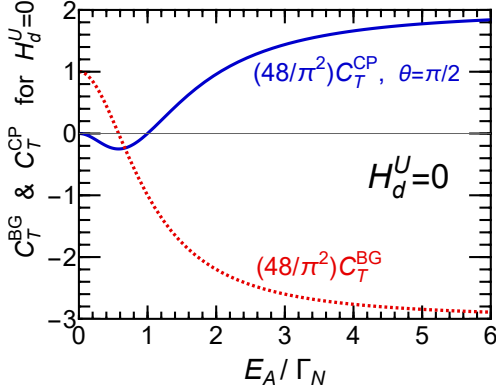


FIG. 3. Coefficients C_T^{BG} and C_T^{CP} for noninteracting electrons ($H_d^U = 0$), plotted as functions of E_A/Γ_N for the Bogoliubov angle $\theta = \pi/2$.

correlations vanish. However, the diagonal components, $\chi_{\sigma\sigma}$ and $\chi_{\sigma\sigma\sigma}^{[3]}$, remain finite, reflecting the Pauli exclusion principle acting on Bogoliubov quasiparticles with the same spin σ . These diagonal components can be derived from derivatives of the noninteracting phase shift $\delta_0 = \cot^{-1}(E_A/\Gamma_N)$ with respect to E_A :

$$\chi_{\uparrow\uparrow}^0 \equiv \frac{\sin^2 \delta_0}{\pi \Gamma_N} = \frac{1}{\pi} \frac{\Gamma_N}{E_A^2 + \Gamma_N^2}, \quad (3.19)$$

$$\Theta_T^{\text{BG}} \xrightarrow{H_d^U \rightarrow 0} \frac{\sin 2\delta_0}{2\pi \left\{ \chi_{\uparrow\uparrow}^0 \right\}^2} \frac{\partial \chi_{\uparrow\uparrow}^0}{\partial E_A} = \frac{-2E_A^2}{E_A^2 + \Gamma_N^2}, \quad (3.20)$$

$$\Theta_T^{\text{CP}} \xrightarrow{H_d^U \rightarrow 0} -\frac{\sin 4\delta_0}{4\pi \left\{ \chi_{\uparrow\uparrow}^0 \right\}^2} \frac{\partial \chi_{\uparrow\uparrow}^0}{\partial E_A} = \frac{2E_A^2 (E_A^2 - \Gamma_N^2)}{\left(E_A^2 + \Gamma_N^2 \right)^2}. \quad (3.21)$$

Figure 3 demonstrates the behavior of C_T^{BG} and C_T^{CP} for $\theta = \pi/2$ in the noninteracting case $H_d^U = 0$, for which the Fermi-liquid energy scale and the Wilson ratio are given by $T_0^* = 1/(4\chi_{\uparrow\uparrow}^0)$ and $R - 1 \rightarrow 0$, respectively. The Cooper-pair contribution C_T^{CP} , which is solely determined by the three-body correlation Θ_T^{CP} , takes negative values in the range $0 < E_A < \Gamma_N$, as the phase shift δ_0 varies from $\pi/2$ to $\pi/4$, reflecting the sign of $\sin 4\delta_0$. In contrast, the Bogoliubov-quasiparticle contribution C_T^{BG} decreases monotonically as E_A increases.

2. NRG approach to interacting Bogoliubov quasiparticles

In order to clarify how the Coulomb interaction affects the coefficients C_T^{CP} and C_T^{BG} , we calculate the correlation functions of the Bogoliubov quasiparticles, δ_σ , $\chi_{\sigma_1\sigma_2}$, and $\chi_{\sigma_1\sigma_2\sigma_3}^{[3]}$ as functions of E_A/U and $U/(\pi\Gamma_N)$, by applying the NRG approach [102–104] to the effective Hamiltonian \mathcal{H}_{eff} . We choose the discretization parameter as $\Lambda = 2.0$, $\Gamma_N/D = 1/(100\pi)$, and typically

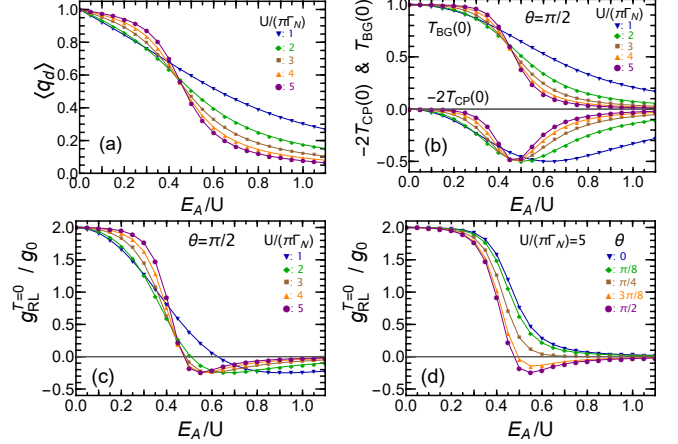


FIG. 4. Phase shift and transmission probabilities at $T = 0$ plotted as functions of E_A/U . (a): Occupation number of Bogoliubov quasiparticles, $\langle q_d \rangle = 2\delta/\pi$. (b): Transmission probability of Bogoliubov quasiparticles, $T_{\text{BG}}(0) = \sin^2 \delta$ and the Cooper-pair contributions, $-2T_{\text{CP}}(0)$ with $T_{\text{CP}}(0) = (1/4) \sin \theta \sin^2 2\delta$. (c) and (d): Nonlocal conductance, $g_{\text{RL}}^{T=0}/(2g_0) = T_{\text{BG}}(0) - 2T_{\text{CP}}(0)$ with $g_0 = \frac{e^2}{h} 4\Gamma_R \Gamma_L / \Gamma_N^2$. The results plotted in panels (a)–(c) are obtained for $U/(\pi\Gamma_N) = 1.0, 2.0, 3.0, 4.0$, and 5.0 . Specifically, the Bogoliubov angle is fixed at $\theta = \pi/2$ for $-2T_{\text{CP}}(0)$ and $g_{\text{RL}}^{T=0}$. For comparison, panel (d) shows the results for $g_{\text{RL}}^{T=0}$ at $\theta = 0, \pi/8, \pi/4, 3\pi/8$, and $\pi/2$, with $U/(\pi\Gamma_N) = 5.0$.

retain 4000 low-lying excited states. Note that the dependence of the conductance on the Bogoliubov angle θ is entirely determined by the superconducting coherence factor $\sin^2 \theta$, as discussed above.

IV. BEHAVIOR OF ANDREEV TRANSPORT AT FINITE TEMPERATURES

In this section, we demonstrate how the three-body correlations between the Bogoliubov quasiparticles contributes to the T^2 term of the Andreev transport at zero magnetic field, $b = 0$. Note that the eigenstates and eigenvalues of the effective Hamiltonian, \mathcal{H}_{eff} , defined in Eq. (2.14), evolve as E_A varies along the radial direction in the ξ_d – Γ_S plane shown in Fig. 2, while they do not depend on the angular coordinate θ .

A. Phase shift and ground-state properties

We first of all discuss the behavior of the phase shift and the nonlocal conductance at zero temperature, $T = 0$, to briefly demonstrate how the leading-order terms vary across the parameter space shown in Fig. 2 [49].

The occupation number of Bogoliubov quasiparticles at the impurity site, $\langle q_d \rangle = 2\delta/\pi$, varies only along the radial direction in the ξ_d – Γ_S plane and is independent of the polar angle θ . In Fig. 4(a), the NRG results for $\langle q_d \rangle$

are plotted as a function of E_A for $U/(\pi\Gamma_N) = 1.0, 2.0, 3.0, 4.0$, and 5.0 . The occupation number $\langle q_{d\sigma} \rangle$ decreases with increasing E_A , particularly around $E_A \simeq U/2$, where a crossover between the Kondo regime and the valence-fluctuation regime of Bogoliubov quasiparticles occurs for strong interactions, $U/(\pi\Gamma_N) \gtrsim 2.0$.

The local superconducting pair correlation $\langle d_{\uparrow}^{\dagger} d_{\downarrow}^{\dagger} + d_{\downarrow} d_{\uparrow} \rangle$ can be deduced from $\langle q_d \rangle$ via Eq. (2.22). In particular, its magnitude is maximized at $\theta = \pi/2$ and is given by $|\langle d_{\uparrow}^{\dagger} d_{\downarrow}^{\dagger} + d_{\downarrow} d_{\uparrow} \rangle| = 1 - \langle q_d \rangle$. Therefore, as E_A increases, the magnitude of the superconducting correlation grows significantly around $E_A \simeq U/2$, and then saturates at its upper bound, 1.0, reflecting the behavior of $\langle q_d \rangle$. Note that at $\theta = \pi/2$, corresponding to $E_A = \Gamma_S$, the occupation number of impurity electrons is fixed at $\langle n_d \rangle = 1$ as a direct consequence of the electron-hole symmetry ($\xi_d = 0$) of the original Hamiltonian H .

The ground-state value of the transmission probability of Bogoliubov quasiparticles, $\mathcal{T}_{\text{BG}}(0) = \sin^2 \delta$, is plotted as a function of E_A in Fig. 4(b). This leading-order term exhibits a clear Kondo ridge at $E_A \lesssim U/2$ for large U , and then decreases for $E_A \gtrsim U/2$, where $\langle q_d \rangle$ rapidly decreases. The corresponding leading-order term of the Cooper-pair transmission probability, $\mathcal{T}_{\text{CP}}(0) = \frac{1}{4} \sin^2 \theta \sin^2 2\delta$, reaches its maximum value at $\delta = \pi/4$, where the local Bogoliubov quasiparticle state is at quarter filling $\langle q_{d\sigma} \rangle = 1/4$. This Cooper-pair contribution is also plotted in Fig. 4(b) for $\theta = \pi/2$, multiplied by a factor of -2 , which arises in the nonlocal conductance as

$$\begin{aligned} g_{RL}^{T=0} &= 2g_0 \left[\mathcal{T}_{\text{BG}}(0) - 2\mathcal{T}_{\text{CP}}(0) \right], \\ &= 2g_0 \sin^2 \delta \left(1 - 2 \sin^2 \theta \cos^2 \delta \right), \end{aligned} \quad (4.1)$$

where $g_0 = \frac{e^2}{h} 4\Gamma_R \Gamma_L / \Gamma_N^2$. The negative sign of this factor reflects the fact that crossed Andreev reflection induces a counterflow, with current flowing from the right lead toward the QD. The NRG results demonstrate that a dip with a depth of $-2\mathcal{T}_{\text{CP}}(0) = -1/2$ appears in the crossover region $E_A \simeq U/2$, and that its width becomes of the order of Γ_N .

Equation (4.1) indicates that the nonlocal conductance becomes negative, $g_{RL}^{T=0} < 0$, in the region where Cooper-pair tunneling dominates, i.e., $\pi/4 < \theta < 3\pi/4$ in the angular direction, and $\cos^2 \delta > 1/(2 \sin^2 \theta)$ in the radial direction. The NRG results shown in Figs. 4(c) and 4(d) clearly demonstrate that the nonlocal conductance decreases from its unitary-limit value, $g_{RL}^{T=0} = 2g_0$, as E_A increases, and becomes negative in the region where the above conditions are satisfied. In particular, for $\theta = \pi/2$, $g_{RL}^{T=0}$ vanishes at the point where the phase shift reaches $\delta = \pi/4$ and exhibits a minimum value of $g_{RL}^{T=0}/g_0 = -1/4$ at $\delta = \pi/6$.

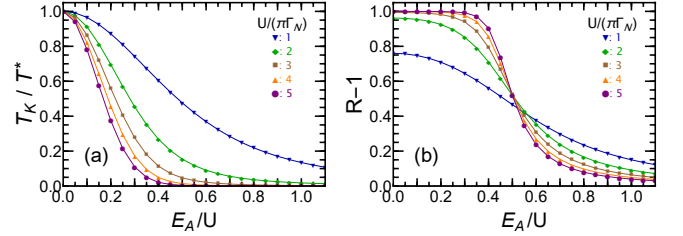


FIG. 5. Inverse of the Fermi-liquid energy scale $1/T^*$ and the Wilson ratio $R - 1$, defined in Eqs. (2.28) and (2.29), plotted as functions of E_A/U for $U/(\pi\Gamma_N) = 1.0, 2.0, 3.0, 4.0$, and 5.0 . Here, $T_K \equiv T^*|_{E_A \rightarrow 0}$ corresponds to the Kondo temperature, which takes the values $T_K/\Gamma_N = 0.494, 0.188, 0.063, 0.020$, and 0.006 , respectively, for these five values of U .

B. Two-body correlations: linear susceptibilities

The Fermi-liquid energy scale and the Wilson ratio, defined by $T^* = 1/(4\chi_{\uparrow\uparrow})$ and $R - 1 = -\chi_{\uparrow\downarrow}/\chi_{\uparrow\uparrow}$, are quantities determined by the two-body correlation function $\chi_{\sigma\sigma'}$. The NRG results for these quantities are shown in Fig. 5 for $U/(\pi\Gamma_N) = 1.0, 2.0, 3.0, 4.0$, and 5.0 . The Kondo temperature, defined at $E_A = 0$ as $T_K \equiv T^*|_{E_A \rightarrow 0}$, takes the values $T_K/\Gamma_N = 0.494, 0.188, 0.063, 0.020$, and 0.006 , respectively, which are much smaller than Γ_N for large U .

Figure 5(a) shows the E_A dependence of $1/T^*$, normalized by T_K . The Fermi-liquid energy scale T^* increases rapidly as E_A moves away from the Fermi level ($E_F = 0$). The Wilson ratio, plotted in Fig. 5(b), exhibits a broad ridge, the height of which reaches the strong-coupling value $R - 1 \simeq 1$ for $U \gtrsim 3.0\pi\Delta$, over a wide Kondo-dominated region $0 \leq E_A \lesssim U/2$ inside the semicircle illustrated in Fig. 2. In contrast, for $E_A \gtrsim U/2$, i.e., in the valence-fluctuation or empty-orbital regime of Bogoliubov quasiparticles, electron correlations become less important and the Wilson ratio approaches $R - 1 \simeq 0$.

C. Three-body FL corrections to CAR

We next discuss the NRG results for the coefficients, C_T^{BG} and C_T^{CP} , which characterize the T^2 terms of the Bogoliubov-quasiparticle and Cooper-pair transmission probabilities, defined in Eqs. (3.13)–(3.18).

As shown in Fig. 6 (a), C_T^{BG} exhibits a positive plateau for large U over the region $E_A \lesssim U/2$, inside the semicircle illustrated in Fig. 2. This behavior originates from the Kondo effect, in which the phase shift is almost locked at $\delta \simeq \pi/2$. In this region, the three-body contribution almost vanishes, $\Theta_T^{\text{BG}} \simeq 0$, reflecting the particle-hole symmetry of Bogoliubov quasiparticles, and the plateau height is determined by the two-body correlations. In contrast, outside the semicircle, for $E_A \gtrsim U/2$, the three-body contribution becomes comparable to the two-body contribution and approaches its lower bound,

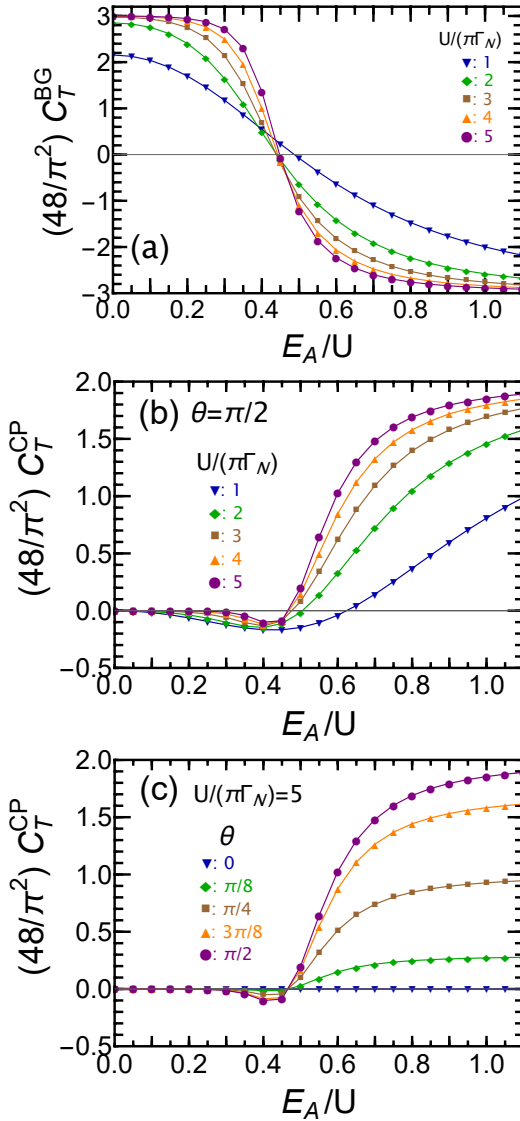


FIG. 6. Coefficients of the T^2 term in the conductance, defined in Eqs. (3.13)–(3.18), are plotted as functions of E_A/U for $U/(\pi\Gamma_N) = 1.0, 2.0, 3.0, 4.0$, and 5.0 , with the Bogoliubov angle fixed at $\theta = \pi/2$. Panels (a) and (b) show C_T^{BG} and C_T^{CP} , which represent the contributions from Bogoliubov-quasiparticle tunneling, $\mathcal{T}_{\text{BG}}(T)$, and Cooper-pair tunneling, $\mathcal{T}_{\text{CP}}(T)$, respectively. The bottom panel (c) demonstrates the $\sin^2 \theta$ dependence of C_T^{CP} , for $\theta = 0, \pi/8, \pi/4, 3\pi/8$, and $\pi/2$, with $U/(\pi\Gamma_N) = 5.0$.

$\Theta_T^{\text{BG}} \xrightarrow{E_A \rightarrow \infty} -2$, while C_T^{BG} also becomes negative and approaches $(48/\pi^2)C_T^{\text{BG}} \xrightarrow{E_A \rightarrow \infty} -3$. Note that the expression for C_T^{BG} , given in Eqs. (3.15) and (3.16), is identical to that for normal electrons tunneling through an N/QD/N junction [85–89].

Figures 6(b) and 6(c) show the coefficient C_T^{CP} of the T^2 term in the Cooper-pair transmission probability. At zero magnetic field, as mentioned above, the Cooper-pair contribution is determined solely by the three-body correlations as shown in Eq. (3.17), namely, $(48/\pi^2)C_T^{\text{CP}} =$

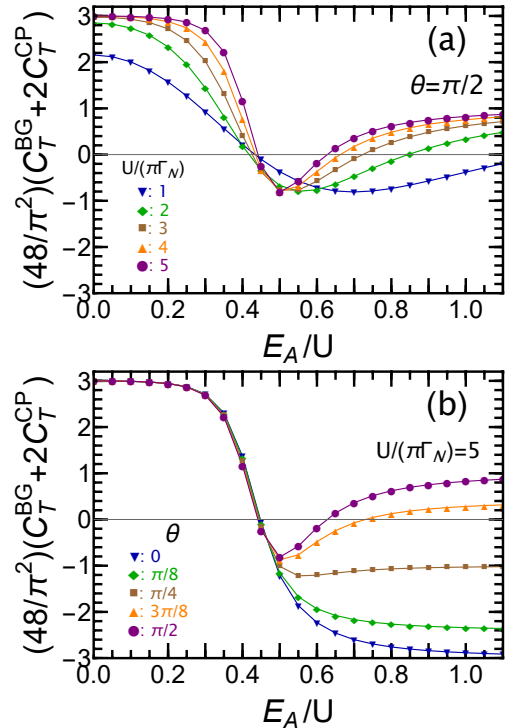


FIG. 7. Coefficient of the T^2 term in the nonlocal conductance g_{RL} , defined in Eq. (3.3), is plotted as a function of E_A/U . This coefficient, $C_T^{\text{BG}} + 2C_T^{\text{CP}}$, arises from the combination $\mathcal{T}_{\text{BG}}(T) - 2\mathcal{T}_{\text{CP}}(T)$, as described in Eqs. (3.13) and (3.14). Upper panel (a): results for $U/(\pi\Gamma_N) = 1.0, 2.0, 3.0, 4.0$, and 5.0 , with $\theta = \pi/2$. Lower panel (b): results for $\theta = 0, \pi/8, \pi/4, 3\pi/8$, and $\pi/2$, with $U/(\pi\Gamma_N) = 5.0$.

$\Theta_T^{\text{CP}} \sin^2 \theta$. Therefore, this Cooper-pair contribution to the T^2 term almost vanishes, $C_T^{\text{CP}} \simeq 0$, over the region $E_A \lesssim U/2$, where the Bogoliubov quasiparticles exhibit genuine ($E_A = 0$) or emergent particle-hole symmetry. In the crossover region $E_A \simeq U/2$, the coefficient C_T^{CP} takes a negative minimum and changes sign at the quarter-filling point $\langle q_d \rangle = 1/2$, reflecting the factor $\sin 4\delta$ inherent in Θ_T^{CP} . The coefficient C_T^{CP} increases for $E_A \gtrsim U/2$, in the region where the superconducting pair correlation, $|\langle d_{\uparrow}^{\dagger} d_{\downarrow}^{\dagger} + d_{\downarrow} d_{\uparrow} \rangle| = (1 - \langle q_d \rangle) \sin \theta$, is enhanced [see Fig. 4 (a) for the behavior of $\langle q_d \rangle$]. It asymptotically approaches the upper bound, which is determined by the coherence factor $\sin^2 \theta$ and by the three-body correlation Θ_T^{CP} approaching its noninteracting value:

$$\Theta_T^{\text{CP}} \xrightarrow{E_A \rightarrow \infty} 2. \quad (4.2)$$

The coefficient C_T^{CP} is maximized at $\theta = \pi/2$, which corresponds to $\xi_d = 0$, and varies with the angle θ , as demonstrated in Fig. 6(c) for $U/(\pi\Gamma_N) = 5.0$.

Figure 7 shows the NRG results for the T^2 term of the nonlocal conductance g_{RL} , defined in Eq. (3.3), which

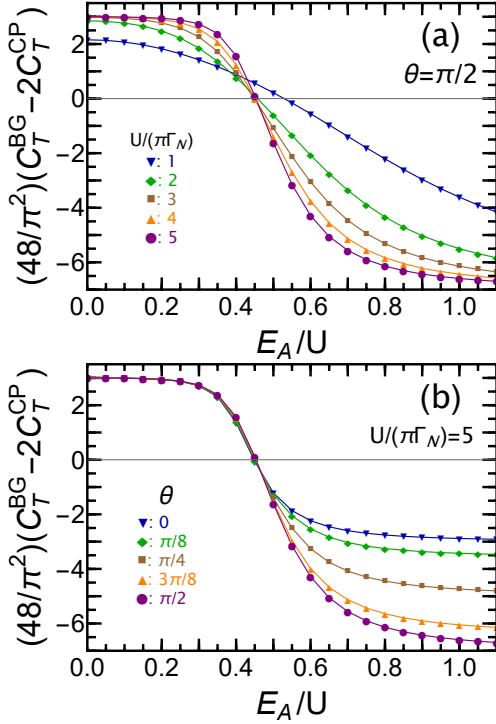


FIG. 8. Coefficient of the T^2 term of the local conductance g_{LL} , shown in Eq. (4.5), is plotted as a function of E_A/U for symmetric tunnel coupling $\Gamma_L = \Gamma_R$. Upper panel (a): results for $U/(\pi\Gamma_N) = 1.0, 2.0, 3.0, 4.0$, and 5.0 , with $\theta = \pi/2$. Lower panel (b): results for $\theta = 0, \pi/8, \pi/4, 3\pi/8$, and $\pi/2$, with $U/(\pi\Gamma_N) = 5.0$.

can also be expressed in the following form:

$$g_{RL} = g_{RL}^{T=0} - 2g_0 \left(C_T^{\text{BG}} + 2C_T^{\text{CP}} \right) \left(\frac{\pi T}{T^*} \right)^2. \quad (4.3)$$

The coefficient $C_T^{\text{BG}} + 2C_T^{\text{CP}}$ depends on the coherence factor, $\sin^2 \theta$, which enters through the Cooper-pairing contribution C_T^{CP} . The Bogoliubov-quasiparticle contribution C_T^{BG} dominates the T^2 term of g_{RL} over the region $E_A \lesssim U/2$ since C_T^{CP} almost vanishes or remains very small in this region, particularly for large U . In contrast, for $E_A \gtrsim U/2$, i.e., outside the semicircle illustrated in Fig. 2, the Cooper-pair contribution C_T^{CP} becomes comparable to C_T^{BG} , particularly in the angular range $\pi/4 \lesssim \theta \lesssim 3\pi/4$. More specifically, the coefficient $C_T^{\text{BG}} + 2C_T^{\text{CP}}$ converges to the following value in the limit $E_A \rightarrow \infty$:

$$\frac{4}{\pi^2} \left(C_T^{\text{BG}} + 2C_T^{\text{CP}} \right) \xrightarrow{E_A \rightarrow \infty} -3 + 4 \sin^2 \theta, \quad (4.4)$$

and it remains positive for $\pi/3 < \theta < 2\pi/3$. This coefficient also exhibits a negative minimum in the crossover region $E_A \simeq U/2$, particularly for large U and $\theta \simeq \pi/2$.

Similarly, the T^2 term in the local conductance g_{LL} , defined in Eq. (3.5), can be expressed in the following

form for $b = 0$:

$$g_{LL} = g_{LL}^{T=0} - 2g_0 \left(C_T^{\text{BG}} - \frac{2\Gamma_L}{\Gamma_R} C_T^{\text{CP}} \right) \left(\frac{\pi T}{T^*} \right)^2, \quad (4.5)$$

$$g_{LL}^{T=0} = 2g_0 \sin^2 \delta \left(1 + \frac{2\Gamma_L}{\Gamma_R} \sin^2 \theta \cos^2 \delta \right). \quad (4.6)$$

Figure 8 shows the coefficient of the T^2 term of g_{LL} for a symmetric junction $\Gamma_L = \Gamma_R$. In contrast to the T^2 term of nonlocal conductance g_{RL} discussed above, the coefficient for the local conductance g_{LL} exhibits a monotonic dependence on E_A , since the Bogoliubov-quasiparticle contribution and the Cooper-pairing contribution add constructively to g_{LL} . The contributions from C_T^{BG} and C_T^{CP} can also be experimentally extracted by measuring the T^2 terms of both g_{RL} and g_{LL} .

V. MICROSCOPIC FERMI-LIQUID THEORY FOR THE T^2 ANDREEV TRANSPORT

In this section, we provide an outline of the derivation of the conductance up to order T^2 , leaving the additional details required for a complete proof to Appendix B.

A. Nambu–Keldysh formalism

We use the spinor representation for the electron operators, ψ_d and ψ_j for $j = L, R$, defined with respect to the Nambu pseudo-spin space:

$$\psi_d = \begin{pmatrix} \psi_{d,1} \\ \psi_{d,2} \end{pmatrix} \equiv \begin{pmatrix} d_\uparrow \\ d_\downarrow^\dagger \end{pmatrix}, \quad (5.1)$$

$$\psi_j = \begin{pmatrix} \psi_{j,1} \\ \psi_{j,2} \end{pmatrix} \equiv \int_{-D}^D d\epsilon \sqrt{\rho_c} \begin{pmatrix} c_{\epsilon,j,\uparrow} \\ -c_{-\epsilon,j,\downarrow}^\dagger \end{pmatrix}. \quad (5.2)$$

In the following, we assign the label p ($= d, L, R$) to spatial configurations, ζ ($= 1, 2$) to the Nambu spinor components, and ν ($= -, +$) to the Keldysh Green's functions [65, 100, 101], defined with respect to the nonequilibrium steady state under finite bias voltages eV :

$$G_{pp';\zeta\zeta'}^{--}(t, t') \equiv -i \langle T \psi_{p,\zeta}(t) \psi_{p',\zeta'}^\dagger(t') \rangle_V, \quad (5.3a)$$

$$G_{pp';\zeta\zeta'}^{++}(t, t') \equiv -i \langle \tilde{T} \psi_{p,\zeta}(t) \psi_{p',\zeta'}^\dagger(t') \rangle_V, \quad (5.3b)$$

$$G_{pp';\zeta\zeta'}^{+-}(t, t') \equiv -i \langle \psi_{p,\zeta}(t) \psi_{p',\zeta'}^\dagger(t') \rangle_V, \quad (5.3c)$$

$$G_{pp';\zeta\zeta'}^{-+}(t, t') \equiv i \langle \psi_{p',\zeta'}^\dagger(t') \psi_{p,\zeta}(t) \rangle_V. \quad (5.3d)$$

Here, T and \tilde{T} are the time-ordering and anti-time-ordering operators, respectively. These Keldysh Green's functions are linearly dependent and can be expressed in terms of three independent components, for instance, the retarded G^r , the advanced G^a , and the symmetrized G^K

Green's functions:

$$G^r = G^{--} - G^{-+}, \quad G^a = G^{--} - G^{+-}, \quad (5.4a)$$

$$G^K \equiv G^{+-} + G^{-+} = G^{--} + G^{++}. \quad (5.4b)$$

The Fourier transform of the Green's function, defined with respect to the steady state, becomes a function of a single frequency ω :

$$G_{pp';\zeta\zeta'}^{\nu\nu'}(\omega) = \int_{-\infty}^{\infty} dt e^{i\omega t} G_{pp';\zeta\zeta'}^{\nu\nu'}(t, 0). \quad (5.5)$$

We use 2×2 matrices to treat the components in the Nambu space,

$$G_{pp'}^{\nu\nu'} = \begin{pmatrix} G_{pp';11}^{\nu\nu'} & G_{pp';12}^{\nu\nu'} \\ G_{pp';21}^{\nu\nu'} & G_{pp';22}^{\nu\nu'} \end{pmatrix}, \quad (5.6)$$

and also 4×4 matrices including all Keldysh components:

$$\hat{G}_{pp'} = \begin{pmatrix} G_{pp'}^{--} & G_{pp'}^{-+} \\ G_{pp'}^{+-} & G_{pp'}^{++} \end{pmatrix}, \quad \hat{\rho}_3 = \begin{pmatrix} \mathbf{1} & \mathbf{0} \\ \mathbf{0} & -\mathbf{1} \end{pmatrix}. \quad (5.7)$$

Here, $\mathbf{1}$ and $\mathbf{0}$ are the 2×2 unit and zero matrices, respectively. We will also use the Pauli matrices:

$$\tau_1 = \begin{pmatrix} 0 & 1 \\ 1 & 0 \end{pmatrix}, \quad \tau_2 = \begin{pmatrix} 0 & -i \\ i & 0 \end{pmatrix}, \quad \tau_3 = \begin{pmatrix} 1 & 0 \\ 0 & -1 \end{pmatrix}. \quad (5.8)$$

B. Green's function for the isolated normal leads

For isolated normal leads disconnected from the dot, the retarded and advanced Green's functions of the conduction electrons ψ_j take the following form for small frequency $|\omega| \ll D$:

$$g_j^r(\omega) = -i\pi\rho_c \mathbf{1}, \quad g_j^a(\omega) = i\pi\rho_c \mathbf{1}, \quad (5.9)$$

Correspondingly, the lesser g_j^{-+} and greater g_j^{+-} Green's functions are given by

$$g_j^{-+}(\omega) = i2\pi\rho_c \mathbf{f}_j(\omega), \quad (5.10)$$

$$g_j^{+-}(\omega) = -i2\pi\rho_c [\mathbf{1} - \mathbf{f}_j(\omega)]. \quad (5.11)$$

Here, $\mathbf{f}_j(\omega)$ is a diagonal matrix describing the distribution functions for electrons (e) and holes (h),

$$\mathbf{f}_j(\omega) \equiv \begin{pmatrix} f_j^{(e)}(\omega) & 0 \\ 0 & f_j^{(h)}(\omega) \end{pmatrix}, \quad (5.12)$$

where $f_j^{(e)}(\omega) \equiv f(\omega - \mu_j^e)$ and $f_j^{(h)}(\omega) \equiv f(\omega - \mu_j^h)$, with $f(\omega) = [e^{\omega/T} + 1]^{-1}$. The bias voltage V_j applied to the normal lead on j ($= L, R$) shifts the chemical potentials for electrons and holes such that

$$\mu_j^e = -\mu_j^h = eV_j. \quad (5.13)$$

Including the causal component $g_j^{--} = g_j^{-+} + g_j^r$ and its counterpart $g_j^{++} = g_j^{+-} - g_j^r$, the Keldysh Green's functions for isolated leads can be expressed in the 4×4 matrix form:

$$\mathbf{g}_j(\omega) = \begin{bmatrix} g_j^{--}(\omega) & g_j^{-+}(\omega) \\ g_j^{+-}(\omega) & g_j^{++}(\omega) \end{bmatrix}. \quad (5.14)$$

The tunnel coupling v_j gives rise not only to level broadening but also to a nonequilibrium distribution in the impurity level, which can be described by the following noninteracting Nambu–Keldysh self-energy:

$$\hat{\Sigma}_0(\omega) = \begin{bmatrix} \Sigma_0^{--}(\omega) & \Sigma_0^{-+}(\omega) \\ \Sigma_0^{+-}(\omega) & \Sigma_0^{++}(\omega) \end{bmatrix} \equiv \sum_{j=L,R} v_j^2 \hat{\rho}_3 \hat{g}_j(\omega) \hat{\rho}_3. \quad (5.15)$$

The lesser Σ_0^{-+} and greater Σ_0^{+-} components depend on the distribution function \mathbf{f}_j :

$$\Sigma_0^{-+}(\omega) = -2i \sum_{j=L,R} \Gamma_j \mathbf{f}_j(\omega), \quad (5.16)$$

$$\Sigma_0^{+-}(\omega) = 2i \sum_{j=L,R} \Gamma_j [\mathbf{1} - \mathbf{f}_j(\omega)]. \quad (5.17)$$

Thus, the components $\Sigma_0^{--} = \Sigma_0^r - \Sigma_0^{-+}$ and $\Sigma_0^{++} = -\Sigma_0^r - \Sigma_0^{+-}$ also depend on the distribution function \mathbf{f}_j , while the retarded component does not:

$$\Sigma_0^r = -i(\Gamma_L + \Gamma_R) \mathbf{1}. \quad (5.18)$$

Similarly, the symmetrized (Keldysh) component of the noninteracting self-energy, $\Sigma_0^K \equiv -\Sigma_0^{-+} - \Sigma_0^{+-}$, is given by

$$\Sigma_0^K(\omega) = -2i \sum_{j=L,R} \Gamma_j [\mathbf{1} - 2\mathbf{f}_j(\omega)]. \quad (5.19)$$

The weighted sum of \mathbf{f}_L and \mathbf{f}_R plays an essential role in the transport properties, and its matrix elements represent the nonequilibrium distribution functions for particles $f_{\text{eff}}^{(e)}(\omega)$ and holes $f_{\text{eff}}^{(h)}(\omega)$:

$$\mathbf{f}_{\text{eff}}(\omega) \equiv \sum_{j=L,R} \frac{\Gamma_j \mathbf{f}_j(\omega)}{\Gamma_L + \Gamma_R} = \begin{pmatrix} f_{\text{eff}}^{(e)}(\omega) & 0 \\ 0 & f_{\text{eff}}^{(h)}(\omega) \end{pmatrix}, \quad (5.20)$$

$$f_{\text{eff}}^{(s)}(\omega) = \frac{\Gamma_L f_L^{(s)}(\omega) + \Gamma_R f_R^{(s)}(\omega)}{\Gamma_L + \Gamma_R}, \quad s = e, h. \quad (5.21)$$

Note that, at equilibrium $eV_L = eV_R = 0$, the distribution-function matrices $\mathbf{f}_j(\omega)$ and the noninteracting self-energy $\Sigma_0^{\nu\nu'}$ become proportional to the unit matrix:

$$\mathbf{f}_j(\omega) \xrightarrow{eV_j \rightarrow 0} f(\omega) \mathbf{1}, \quad \Sigma_0^{\nu\nu'}(\omega) \Big|_{eV \rightarrow 0} \propto \mathbf{1}. \quad (5.22)$$

C. Impurity Green's function at finite bias voltages

We next consider the nonequilibrium Green's function for a quantum dot connected to normal and superconducting leads. Specifically, we set the chemical potential for the SC lead μ_S at the Fermi level ($\mu_S \equiv 0$) and consider the large superconducting-gap limit $|\Delta_S| \rightarrow \infty$, as mentioned in Sec. II B. In this limit, the SC proximity effects penetrating into the impurity site can be described faithfully by an effective Hamiltonian \mathcal{H}_{eff} , the free-impurity part of which can be expressed in the following form:

$$\begin{aligned} \xi_d(n_d - 1) - b(n_{d\uparrow} - n_{d\downarrow}) + \Gamma_S(d_{d\uparrow}^\dagger d_{d\downarrow}^\dagger + d_{d\downarrow} d_{d\uparrow}) \\ = \psi_d^\dagger \mathcal{H}_d^0 \psi_d + b, \\ \mathcal{H}_d^0 \equiv \begin{pmatrix} \xi_d & \Gamma_S \\ \Gamma_S & -\xi_d \end{pmatrix} - b \mathbf{1}. \end{aligned} \quad (5.23)$$

The Keldysh Green's function for the isolated impurity site, disconnected from the normal leads, is given by

$$\{\hat{\mathbf{g}}_{dd}(\omega)\}^{-1} = \begin{bmatrix} \omega \mathbf{1} - \mathcal{H}_d^0 & \mathbf{0} \\ \mathbf{0} & -(\omega \mathbf{1} - \mathcal{H}_d^0) \end{bmatrix}. \quad (5.24)$$

The bias dependence enters through the tunnel couplings between the impurity and normal leads, which can be taken into account using the Dyson equation:

$$\{\hat{\mathbf{G}}_0(\omega)\}^{-1} = \{\hat{\mathbf{g}}_{dd}(\omega)\}^{-1} - \hat{\Sigma}_0(\omega). \quad (5.25)$$

Similarly, electron correlations arising from H_d^U , defined in Eq. (2.3), enter through the interacting self-energy $\hat{\Sigma}_U(\omega)$ in the Nambu–Keldysh formalism,

$$\{\hat{\mathbf{G}}_{dd}(\omega)\}^{-1} = \{\hat{\mathbf{G}}_0(\omega)\}^{-1} - \hat{\Sigma}_U(\omega), \quad (5.26)$$

$$\hat{\Sigma}_{\text{tot}}(\omega) = \hat{\Sigma}_0(\omega) + \hat{\Sigma}_U(\omega). \quad (5.27)$$

From Eq. (5.26), it follows that the symmetrized Green's function $\mathbf{G}_{dd}^K \equiv \mathbf{G}_{dd}^{+-} + \mathbf{G}_{dd}^{-+}$ can be factorized as

$$\mathbf{G}_{dd}^K(\omega) = \mathbf{G}_{dd}^r(\omega) \Sigma_{\text{tot}}^K(\omega) \mathbf{G}_{dd}^a(\omega), \quad (5.28)$$

where $\Sigma_{\text{tot}}^K = -\Sigma_{\text{tot}}^{+-} - \Sigma_{\text{tot}}^{-+}$. Similar relations also hold for the lesser and greater Green's functions,

$$\mathbf{G}_{dd}^{-+}(\omega) = -\mathbf{G}_{dd}^r(\omega) \Sigma_{\text{tot}}^{-+}(\omega) \mathbf{G}_{dd}^a(\omega), \quad (5.29)$$

$$\mathbf{G}_{dd}^{+-}(\omega) = -\mathbf{G}_{dd}^r(\omega) \Sigma_{\text{tot}}^{+-}(\omega) \mathbf{G}_{dd}^a(\omega). \quad (5.30)$$

D. Non-local Green's functions

The non-local Green's functions between the impurity site and the normal leads ($j = L, R$) satisfy the following relations:

$$\hat{\mathbf{G}}_{jd}(\omega) = -v_j \hat{\mathbf{g}}_j(\omega) \hat{\rho}_3 \hat{\mathbf{G}}_{dd}(\omega), \quad (5.31)$$

$$\hat{\mathbf{G}}_{dj}(\omega) = -v_j \hat{\mathbf{G}}_{dd} \hat{\rho}_3 \hat{\mathbf{g}}_j(\omega). \quad (5.32)$$

The expectation values of the currents, $I_{j,\sigma} \equiv \langle \hat{I}_{j,\sigma} \rangle$, for $j = L, R$, defined in Eqs. (2.8) and (2.9), can be expressed in terms of the non-local lesser and greater Green's functions,

$$I_{j,\uparrow} = \frac{e}{h} \int_{-\infty}^{\infty} d\omega \eta_j v_j \left[\mathbf{G}_{dj}^{-+}(\omega) - \mathbf{G}_{jd}^{-+}(\omega) \right]_{11}, \quad (5.33)$$

$$I_{j,\downarrow} = -\frac{e}{h} \int_{-\infty}^{\infty} d\omega \eta_j v_j \left[\mathbf{G}_{dj}^{+-}(\omega) - \mathbf{G}_{jd}^{+-}(\omega) \right]_{22}, \quad (5.34)$$

where $\eta_R = 1$, and $\eta_L = -1$. The (1,1) and (2,2) components of matrices on the right-hand sides of these equations represent the currents carried by electrons with spin $\sigma = \uparrow$ and \downarrow , respectively. These matrix parts can also be expressed in terms of the impurity Green's function by using Eqs. (5.28)–(5.32),

$$\begin{aligned} v_j \left[\mathbf{G}_{dj}^{-+} - \mathbf{G}_{jd}^{-+} \right]_{11} \\ = -i\Gamma_j \left[\mathbf{G}_{dd}^K - \left(1 - 2f_j^{(e)} \right) \left\{ \mathbf{G}_{dd}^r - \mathbf{G}_{dd}^a \right\} \right]_{11} \\ = -i\Gamma_j \left[\mathbf{G}_{dd}^r \Pi_{\text{tot}}^{j;(e)} \mathbf{G}_{dd}^a \right]_{11}, \end{aligned} \quad (5.35)$$

$$\begin{aligned} v_j \left[\mathbf{G}_{dj}^{+-} - \mathbf{G}_{jd}^{+-} \right]_{22} \\ = -i\Gamma_j \left[\mathbf{G}_{dd}^K - \left(1 - 2f_j^{(h)} \right) \left\{ \mathbf{G}_{dd}^r - \mathbf{G}_{dd}^a \right\} \right]_{22} \\ = -i\Gamma_j \left[\mathbf{G}_{dd}^r \Pi_{\text{tot}}^{j;(h)} \mathbf{G}_{dd}^a \right]_{22}. \end{aligned} \quad (5.36)$$

Here, $\Pi_{\text{tot}}^{j;(e)}$ and $\Pi_{\text{tot}}^{j;(h)}$ are given by linear combinations of the self-energy matrices which are purely imaginary and depend on j ($= L, R$) through the Fermi distribution functions $f_j^{(e)}$ and $f_j^{(h)}$ as follows:

$$\Pi_{\text{tot}}^{j;(e)} \equiv \Sigma_{\text{tot}}^K - \left(1 - 2f_j^{(e)} \right) \left(\Sigma_{\text{tot}}^{-+} - \Sigma_{\text{tot}}^{+-} \right), \quad (5.37)$$

$$\Pi_{\text{tot}}^{j;(h)} \equiv \Sigma_{\text{tot}}^K - \left(1 - 2f_j^{(h)} \right) \left(\Sigma_{\text{tot}}^{-+} - \Sigma_{\text{tot}}^{+-} \right). \quad (5.38)$$

Note that $\Sigma_{\text{tot}}^{-+} - \Sigma_{\text{tot}}^{+-} = \Sigma_{\text{tot}}^r - \Sigma_{\text{tot}}^a$. Thus, the average currents, Eqs. (5.33) and (5.34), can also be expressed in the following forms,

$$I_{j,\uparrow} = \frac{e}{h} \int_{-\infty}^{\infty} d\omega (-i\eta_j \Gamma_j) \left[\mathbf{G}_{dd}^r \Pi_{\text{tot}}^{j;(e)} \mathbf{G}_{dd}^a \right]_{11}, \quad (5.39)$$

$$I_{j,\downarrow} = -\frac{e}{h} \int_{-\infty}^{\infty} d\omega (-i\eta_j \Gamma_j) \left[\mathbf{G}_{dd}^r \Pi_{\text{tot}}^{j;(h)} \mathbf{G}_{dd}^a \right]_{22}. \quad (5.40)$$

At equilibrium $eV = 0$, the symmetrized Keldysh self-energy Σ_{tot}^K can be expressed in terms of the imaginary part of the retarded self-energy as

$$\Sigma_{\text{tot}}^K \Big|_{eV=0} = (1 - 2f) \left(\Sigma_{\text{tot}}^r - \Sigma_{\text{tot}}^a \right) \Big|_{eV=0}. \quad (5.41)$$

Thus, the integrands in Eqs. (5.39) and (5.40) vanish at $eV = 0$, since the first and second terms of $\Pi_{\text{tot}}^{j;(s)}$, shown

on the right-hand sides of Eqs. (5.37) and (5.38), cancel each other out,

$$\Pi_{\text{tot}}^{j;(s)} \xrightarrow{eV \rightarrow 0} 0, \quad s = e, h. \quad (5.42)$$

Therefore, the linear terms in eV of the currents $I_{j,\uparrow}$ and that of $I_{j,\downarrow}$ arise from $\Pi_{\text{tot}}^{j;(e)}$ and $\Pi_{\text{tot}}^{j;(h)}$, respectively. Consequently, in order to calculate the linear-response currents, the Green's functions $\mathbf{G}_{dd}^r(\omega)$ and $\mathbf{G}_{dd}^a(\omega)$ appearing in Eqs. (5.39) and (5.40) can be replaced by their equilibrium values evaluated at $eV = 0$, the explicit forms of which are summarized in Appendix A.

The self-energy part $\Pi_{\text{tot}}^{j;(s)}$ for $s = e, h$ can be decomposed into two parts, $\Pi_0^{j;(s)}$ and $\Pi_U^{j;(s)}$, which represent the contributions from the noninteracting self-energy and the interacting self-energy, respectively, as

$$\Pi_{\text{tot}}^{j;(s)} = \Pi_0^{j;(s)} + \Pi_U^{j;(s)}, \quad (5.43)$$

$$\Pi_0^{j;(s)} \equiv \Sigma_0^K - \left(1 - 2f_j^{(s)}\right) \left(\Sigma_0^{-+} - \Sigma_0^{+-}\right), \quad (5.44)$$

$$\Pi_U^{j;(s)} \equiv \Sigma_U^K - \left(1 - 2f_j^{(s)}\right) \left(\Sigma_U^{-+} - \Sigma_U^{+-}\right), \quad (5.45)$$

Correspondingly, the average current $I_{j,\sigma}$ can also be decomposed into two parts, $I_{j,\sigma}^{(0)}$ and $I_{j,\sigma}^{(U)}$, which represent the contributions from $\Pi_0^{j;(s)}$ and $\Pi_U^{j;(s)}$, respectively,

$$I_{j,\sigma} = I_{j,\sigma}^{(0)} + I_{j,\sigma}^{(U)}. \quad (5.46)$$

The linear-response contribution to $I_{j,\sigma}^{(0)}$ arises from the noninteracting part $\Pi_0^{j;(s)}$, which can be expressed in the following form using Eqs. (5.16)–(5.19):

$$\left. \frac{\partial \Pi_0^{j';(s)}}{\partial eV_j} \right|_{eV=0} = 4i \left[\Gamma_j \boldsymbol{\tau}_3 - \eta^{(s)} \Gamma_N \delta_{jj'} \mathbf{1} \right] \left(-\frac{\partial f(\omega)}{\partial \omega} \right), \quad (5.47)$$

where $\eta^{(s)}$ is a sign factor defined by $\eta^{(e)} = 1$ and $\eta^{(h)} = -1$, and $\Gamma_N \equiv \Gamma_L + \Gamma_R$.

The interacting counterpart $\Pi_U^{j;(s)}$ exhibits ω^2 and T^2 dependence at low energies, reflecting the finite lifetime of

the Bogoliubov quasiparticles. We will show more specifically in Sec. V F and Appendix B that the first derivative of $\Pi_U^{j;(s)}$ with respect to eV exhibits the following asymptotic behavior at $eV = 0$:

$$\left[\omega^2 + (\pi T)^2 \right] \left(-\frac{\partial f(\omega)}{\partial \omega} \right). \quad (5.48)$$

Therefore, the linear-response term of $I_{j,\sigma}^{(U)}$, arising from the interacting part $\Pi_U^{j;(s)}$ vanishes at $T = 0$ and is proportional to T^2 at low temperatures. This T^2 dependence arising from $\Pi_U^{j;(s)}$ can be obtained by setting the frequency and temperature to $\omega = T = 0$ in $\mathbf{G}_{dd}^r(\omega)$ and $\mathbf{G}_{dd}^a(\omega)$ appearing on the right-hand side of Eqs. (5.39) and (5.40).

E. Linear-response current $I_{j,\sigma}^{(0)}$ up to order T^2

In order to obtain the T^2 contribution to the conductance arising from $I_{j,\sigma}^{(0)}$, the Green's functions $\mathbf{G}_{dd}^r(\omega)$ and $\mathbf{G}_{dd}^a(\omega)$, appearing in the right-hand sides of Eqs. (5.39) and (5.40), need to be expanded up to terms of order ω^2 and T^2 . This point has been clarified for the diagonal element $G_{\gamma,\sigma}^r(\omega)$ in previous works [86, 88]. It has also been shown that three-body correlations play an essential role in the next-to-leading-order transport in the Fermi-liquid regime. The exact low-energy asymptotic form of the corresponding diagonal retarded self-energy $\Sigma_{\gamma,\sigma}^r(\omega)$ is shown in Appendix A.

We can now calculate $I_{j,\sigma}^{(0)}$ by substituting Eq. (5.47) into Eqs. (5.39) and (5.40), and then performing the Bogoliubov transformation, $\mathcal{U} = e^{-i\frac{\theta}{2}\boldsymbol{\tau}_2}$ defined in Eq. (2.13), which diagonalizes \mathcal{H}_d^0 ,

$$\mathcal{U}^\dagger \mathcal{H}_d^0 \mathcal{U} = E_A \boldsymbol{\tau}_3 - b \mathbf{1}. \quad (5.49)$$

Here, $E_A = \sqrt{\xi_d^2 + \Gamma_S^2}$, $\sin \theta = \frac{\Gamma_S}{E_A}$, $\cos \theta = \frac{\xi_d}{E_A}$, and

$$\mathcal{U}^\dagger \boldsymbol{\tau}_1 \mathcal{U} = \cos \theta \boldsymbol{\tau}_1 + \sin \theta \boldsymbol{\tau}_3, \quad (5.50)$$

$$\mathcal{U}^\dagger \boldsymbol{\tau}_3 \mathcal{U} = -\sin \theta \boldsymbol{\tau}_1 + \cos \theta \boldsymbol{\tau}_3. \quad (5.51)$$

As shown in Eq. (2.18), $\tilde{G}^r(\omega) \equiv \mathcal{U}^\dagger \mathbf{G}_{dd}^r(\omega) \mathcal{U}$ corresponds to the propagators of Bogoliubov quasiparticles: $\tilde{G}_1^r(\omega) = G_{\gamma,\uparrow}^r(\omega)$, and $\tilde{G}_2^r(\omega) = -G_{\gamma,\downarrow}^a(-\omega)$. Using, in addition, the low-energy asymptotic form of the retarded self-energy $\Sigma_{\gamma,\sigma}^r(\omega)$ shown in Appendix A, we obtain the T^2 contribution to conductance arising from $I_{j,\sigma}^{(0)}$,

$$\begin{aligned}
\sum_{\sigma} \frac{\partial I_{j',\sigma}^{(0)}}{\partial V_j} \Big|_{eV=0} &= \frac{e^2}{h} \int_{-\infty}^{\infty} d\omega (-i\eta_{j'}) \Gamma_{j'} \left[\left\{ \mathbf{G}_{dd}^r(\omega) \frac{\partial \mathbf{\Pi}_0^{j';(e)}}{\partial eV_j} \Big|_{eV=0} \mathbf{G}_{dd}^a(\omega) \right\}_{11} - \left\{ \mathbf{G}_{dd}^r(\omega) \frac{\partial \mathbf{\Pi}_0^{j';(h)}}{\partial eV_j} \Big|_{eV=0} \mathbf{G}_{dd}^a(\omega) \right\}_{22} \right] \\
&= \frac{e^2}{h} \int_{-\infty}^{\infty} d\omega \left(-\frac{\partial f}{\partial \omega} \right) \frac{(-4)\eta_{j'}\Gamma_{j'}}{\Gamma_N} \left\{ \delta_{jj'} \Gamma_N^2 \text{Tr}[\mathbf{G}_{dd}^r(\omega) \mathbf{G}_{dd}^a(\omega)] - \frac{\Gamma_j}{\Gamma_N} \Gamma_N^2 \text{Tr}[\mathbf{G}_{dd}^r(\omega) \boldsymbol{\tau}_3 \mathbf{G}_{dd}^a(\omega) \boldsymbol{\tau}_3] \right\} \\
&= \frac{e^2}{h} \frac{(-4)\eta_{j'}\Gamma_{j'}}{\Gamma_N} \left[\left(\delta_{jj'} - \frac{\Gamma_j}{\Gamma_N} \right) \left\{ \sum_{\sigma} \sin^2 \delta_{\sigma} - a_{\text{I}}^{(0)} (\pi T)^2 \right\} + \frac{\Gamma_j}{\Gamma_N} \left\{ \sin^2(\delta_{\uparrow} + \delta_{\downarrow}) + a_{\text{II}}^{(0)} (\pi T)^2 \right\} \sin^2 \theta \right], \tag{5.52}
\end{aligned}$$

where $\eta_R = 1$ and $\eta_L = -1$. The coefficients $a_{\text{I}}^{(0)}$ and $a_{\text{II}}^{(0)}$ are given by

$$\begin{aligned}
a_{\text{I}}^{(0)} &\equiv -\frac{\pi^2}{3} \sum_{\sigma} \left[\cos 2\delta_{\sigma} \chi_{\sigma\sigma}^2 - 4 \sin^2 \delta_{\sigma} \chi_{\uparrow\downarrow}^2 \right. \\
&\quad \left. - \frac{\sin 2\delta_{\sigma}}{2\pi} \left(\chi_{\sigma\sigma\sigma}^{[3]} + \chi_{\sigma\bar{\sigma}\bar{\sigma}}^{[3]} \right) \right], \tag{5.53}
\end{aligned}$$

$$\begin{aligned}
a_{\text{II}}^{(0)} &\equiv \frac{\pi^2}{3} \left[\cos(2\delta_{\uparrow} + 2\delta_{\downarrow}) (\chi_{\uparrow\uparrow} - \chi_{\downarrow\downarrow})^2 - 8 \sin^2(\delta_{\uparrow} + \delta_{\downarrow}) \chi_{\uparrow\downarrow}^2 \right. \\
&\quad \left. - \frac{\sin(2\delta_{\uparrow} + 2\delta_{\downarrow})}{2\pi} \left(\chi_{\uparrow\uparrow\uparrow}^{[3]} + \chi_{\uparrow\uparrow\downarrow}^{[3]} + \chi_{\downarrow\downarrow\uparrow}^{[3]} + \chi_{\downarrow\downarrow\downarrow}^{[3]} \right) \right], \tag{5.54}
\end{aligned}$$

and $\bar{\sigma}$ represents the opposite spin component to σ . To obtain the last line of Eq. (5.52), we have used the diagonal representation of \mathbf{G}_{dd}^r and \mathbf{G}_{dd}^a ,

$$\begin{aligned}
\text{Tr}[\mathbf{G}_{dd}^r(\omega) \mathbf{G}_{dd}^a(\omega)] &= \text{Tr}[\tilde{\mathbf{G}}^r(\omega) \tilde{\mathbf{G}}^a(\omega)] \\
&= |\tilde{G}_1^r(\omega)|^2 + |\tilde{G}_2^r(\omega)|^2, \tag{5.55}
\end{aligned}$$

and

$$\begin{aligned}
\text{Tr}[\mathbf{G}_{dd}^r \boldsymbol{\tau}_3 \mathbf{G}_{dd}^a \boldsymbol{\tau}_3] &= \text{Tr}[\tilde{\mathbf{G}}^r \mathbf{U}^{\dagger} \boldsymbol{\tau}_3 \mathbf{U} \tilde{\mathbf{G}}^a \mathbf{U}^{\dagger} \boldsymbol{\tau}_3 \mathbf{U}] \\
&= \text{Tr}[\tilde{\mathbf{G}}^r (\cos \theta \boldsymbol{\tau}_3 - \sin \theta \boldsymbol{\tau}_1) \tilde{\mathbf{G}}^a (\cos \theta \boldsymbol{\tau}_3 - \sin \theta \boldsymbol{\tau}_1)] \\
&= \text{Tr}[\tilde{\mathbf{G}}^r \boldsymbol{\tau}_3 \tilde{\mathbf{G}}^a \boldsymbol{\tau}_3] \cos^2 \theta + \text{Tr}[\tilde{\mathbf{G}}^r \boldsymbol{\tau}_1 \tilde{\mathbf{G}}^a \boldsymbol{\tau}_1] \sin^2 \theta \\
&= [|\tilde{G}_1^r|^2 + |\tilde{G}_2^r|^2] \cos^2 \theta + [\tilde{G}_1^r \tilde{G}_2^a + \tilde{G}_2^r \tilde{G}_1^a] \sin^2 \theta. \tag{5.56}
\end{aligned}$$

The contribution from the term $\text{Tr}[\mathbf{G}_{dd}^r \mathbf{G}_{dd}^a]$ can be expressed in the following form, using Eqs. (A13) and

(A14):

$$\begin{aligned}
&\int_{-\infty}^{\infty} d\omega \left(-\frac{\partial f(\omega)}{\partial \omega} \right) \Gamma_N^2 \text{Tr}[\mathbf{G}_{dd}^r(\omega) \mathbf{G}_{dd}^a(\omega)] \\
&= \int_{-\infty}^{\infty} d\omega \left(-\frac{\partial f(\omega)}{\partial \omega} \right) \Gamma_N^2 \sum_{\sigma} |G_{\gamma,\sigma}^r(\omega)|^2 \\
&= \sum_{\sigma} \sin^2 \delta_{\sigma} - a_{\text{I}}^{(0)} (\pi T)^2 + O(T^4). \tag{5.57}
\end{aligned}$$

The dependence on the Bogoliubov angle θ arises from the counterpart involving $\text{Tr}[\mathbf{G}_{dd}^r \boldsymbol{\tau}_3 \mathbf{G}_{dd}^a \boldsymbol{\tau}_3]$,

$$\begin{aligned}
&\int_{-\infty}^{\infty} d\omega \left(-\frac{\partial f(\omega)}{\partial \omega} \right) \Gamma_N^2 \left\{ \text{Tr}[\mathbf{G}_{dd}^r(\omega) \mathbf{G}_{dd}^a(\omega)] \right. \\
&\quad \left. - \text{Tr}[\mathbf{G}_{dd}^r(\omega) \boldsymbol{\tau}_3 \mathbf{G}_{dd}^a(\omega) \boldsymbol{\tau}_3] \right\} \\
&= \sin^2 \theta \int_{-\infty}^{\infty} d\omega \left(-\frac{\partial f(\omega)}{\partial \omega} \right) \Gamma_N^2 \left[\sum_{\sigma} |G_{\gamma,\sigma}^r(\omega)|^2 \right. \\
&\quad \left. + G_{\gamma,\uparrow}^r(\omega) G_{\gamma,\downarrow}^r(-\omega) + G_{\gamma,\uparrow}^a(\omega) G_{\gamma,\downarrow}^a(-\omega) \right] \\
&= [\sin^2(\delta_{\uparrow} + \delta_{\downarrow}) + a_{\text{II}}^{(0)} (\pi T)^2] \sin^2 \theta + O(T^4). \tag{5.58}
\end{aligned}$$

Note that the integrals over ω can be evaluated using the relations,

$$\int_{-\infty}^{\infty} d\omega \left(-\frac{\partial f(\omega)}{\partial \omega} \right) = 1, \tag{5.59}$$

$$\int_{-\infty}^{\infty} d\omega \omega^2 \left(-\frac{\partial f(\omega)}{\partial \omega} \right) = \frac{1}{3} (\pi T)^2. \tag{5.60}$$

F. Linear-response current $I_{j,\sigma}^{(U)}$ up to order T^2

We next evaluate the T^2 term in the linear-response current $I_{j,\sigma}^{(U)}$, arising from the interacting parts $\mathbf{\Pi}_U^{j;(e)}$ and

$\Pi_U^{j;(h)}$, which enter Eqs. (5.39) and (5.40), respectively, through Eq. (5.43). Here, we outline the derivation, leaving the full details to Appendix B.

To this end, we rewrite the Coulomb interaction part H_d^U of the Hamiltonian, defined in Eq. (2.3), into several equivalent forms:

$$\begin{aligned} H_d^U &\equiv \frac{U}{2} (n_d - 1)^2 = \frac{U}{2} \left(\tilde{\psi}_{d,1}^\dagger \tilde{\psi}_{d,1} - \tilde{\psi}_{d,2}^\dagger \tilde{\psi}_{d,2} \right)^2 \\ &= \frac{U}{2} \left(\gamma_{d\uparrow}^\dagger \gamma_{d\uparrow} + \gamma_{d\downarrow}^\dagger \gamma_{d\downarrow} - 1 \right)^2. \end{aligned} \quad (5.61)$$

In particular, at finite bias voltages, the Keldysh perturbation theory with respect to H_d^U is most naturally formulated using the second representation in terms of $\tilde{\psi}_{d,1} \equiv \gamma_{d\uparrow}$ and $\tilde{\psi}_{d,2} \equiv \gamma_{d\downarrow}^\dagger$.

The effects of multiple scattering processes caused by H_d^U can be taken into account using the vertex function, as described in Fig. 9. Specifically, the two processes described in Figs. 9 and 10, give rise to the T^2 term in the linear-response current $I_{j,\sigma}^{(U)}$. In the interacting self-energy part $\Pi_U^{j;(s)}$, these two processes can be formulated in terms of the superconducting collision integrals of Bogoliubov quasiparticles shown in Appendix B, leading to an imaginary part of order ω^2 and T^2 , i.e., the same order as the damping rate of quasiparticles in the Fermi-liquid regime. Consequently, the contributions from $\Pi_U^{j;(s)}$ for $s = e, h$ can be expressed in the following form:

$$\begin{aligned} &\left\{ \mathbf{G}_{dd}^r(0) \left. \frac{\partial \Pi_U^{j';(e)}}{\partial eV_j} \right|_{eV=0} \mathbf{G}_{dd}^a(0) \right\}_{11} \\ &= -i \frac{2\pi^2 \chi_{\uparrow\downarrow}^2}{\Gamma_N} \left[\omega^2 + (\pi T)^2 \right] \left(-\frac{\partial f(\omega)}{\partial \omega} \right) \\ &\times \left[\left(\delta_{jj'} - \frac{\Gamma_j}{\Gamma_N} \right) + \frac{2\Gamma_j}{\Gamma_N} \sin^2(\delta_\uparrow + \delta_\downarrow) \sin^2 \theta \right], \end{aligned} \quad (5.62)$$

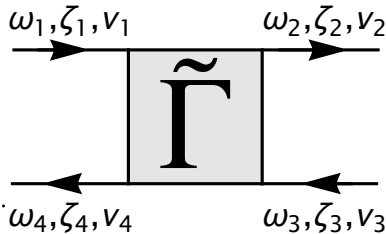


FIG. 9. Keldysh vertex correction $\tilde{\Gamma}_{\zeta_1 \zeta_2; \zeta_3 \zeta_4}^{\nu_1 \nu_2; \nu_3 \nu_4}(\omega_1, \omega_2; \omega_3 \omega_4)$ between Bogoliubov quasiparticles. Here, ζ_i ($= 1, 2$) labels the operators $\tilde{\psi}_{d,1} \equiv \gamma_{d\uparrow}$ and $\tilde{\psi}_{d,2} \equiv \gamma_{d\downarrow}^\dagger$, defined in Eq. (5.61) with respect to the principal axes in the Nambu pseudo-spin space. The superscript ν_i specifies the branches of Keldysh time-loop contour, for which $\nu = -$ and $+$ denote the forward and backward branches, respectively. Frequency conservation requires $\omega_1 + \omega_3 = \omega_2 + \omega_4$.

and

$$\begin{aligned} &- \left\{ \mathbf{G}_{dd}^r(0) \left. \frac{\partial \Pi_U^{j';(h)}}{\partial eV_j} \right|_{eV=0} \mathbf{G}_{dd}^a(0) \right\}_{22} \\ &= \left\{ \mathbf{G}_{dd}^r(0) \left. \frac{\partial \Pi_U^{j';(e)}}{\partial eV_j} \right|_{eV=0} \mathbf{G}_{dd}^a(0) \right\}_{11}. \end{aligned} \quad (5.63)$$

Here, the off-diagonal susceptibility $\chi_{\uparrow\downarrow}$ appears through the Ward identity, $\chi_{\uparrow\downarrow} = -\Gamma_{\uparrow\downarrow; \uparrow\downarrow}^{--}(0, 0; 0, 0) \rho_{d\uparrow} \rho_{d\downarrow}$, which relates the susceptibility to the vertex function of the Bogoliubov quasiparticles, as explained in Appendix A. The T^2 term of the linear-response current $I_{j,\sigma}^{(U)}$ can be obtained by integrating Eq. (5.62) over ω , while setting $\omega = T = 0$ in the Green's functions \mathbf{G}_{dd}^r and \mathbf{G}_{dd}^a appearing in that equation:

$$\begin{aligned} &\left. \frac{\partial I_{j',\sigma}^{(U)}}{\partial V_j} \right|_{eV=0} \\ &= \frac{e^2}{h} (-i\eta_{j'}) \Gamma_{j'} \int_{-\infty}^{\infty} d\omega \left\{ \mathbf{G}_{dd}^r(0) \left. \frac{\partial \Pi_U^{j';(e)}}{\partial eV_j} \right|_{eV=0} \mathbf{G}_{dd}^a(0) \right\}_{11} \\ &= \frac{e^2}{h} (-4\eta_{j'}) \frac{\Gamma_{j'}}{\Gamma_N} \frac{2\pi^2}{3} \chi_{\uparrow\downarrow}^2 (\pi T)^2 \\ &\times \left[\left(\delta_{jj'} - \frac{\Gamma_j}{\Gamma_N} \right) + \frac{2\Gamma_j}{\Gamma_N} \sin^2(\delta_\uparrow + \delta_\downarrow) \sin^2 \theta \right], \end{aligned} \quad (5.64)$$

where $\eta_R = 1$, and $\eta_L = -1$. This result holds for both spin components, $\sigma = \uparrow$ and \downarrow . Consequently, the conductance formula presented in Sec. III follows from $I_{j,\sigma}^{(U)}$ obtained here, combined with the other contribution $I_{j,\sigma}^{(0)}$ given in Eq. (5.52).

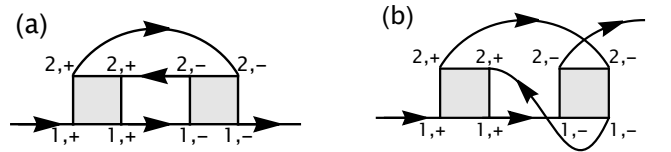


FIG. 10. Feynman diagrams for (a) $\tilde{\Sigma}_{U;11}^{-+}(\omega)$, and (b) $\tilde{\Sigma}_{U;21}^{-+}(\omega)$ which yield the imaginary parts of order ω^2 and T^2 contributing to the linear conductance through $\tilde{\Pi}_U^{j;(s)}$ with s ($= e, h$). The shaded squares represent the scattering amplitudes of quasiparticles, given by the full vertex corrections at $T = eV = 0$: $\tilde{\Gamma}_{12;21}^{--;--}(0, 0; 0, 0) = -\tilde{\Gamma}_{12;21}^{++;++}(0, 0; 0, 0)$. The off-diagonal components ($\zeta \neq \zeta'$) of the scattering amplitude are real and finite.

VI. SUMMARY

We have presented a complete microscopic Fermi-liquid description for crossed Andreev reflection occurring in quantum dots connected to multiple terminals consisting of superconducting and normal leads at finite temperatures, in the the limit of large SC gap, $|\Delta_S| \rightarrow \infty$. Our formulation is based on the Nambu-Keldysh Green's function approach and shows that the T^2 term of the linear conductance can be expressed in terms of the three-body correlation functions $\chi_{\sigma_1\sigma_2\sigma_3}^{[3]}$ in addition to the phase shifts δ_σ , the linear susceptibilities $\chi_{\sigma_1\sigma_2}$, and the Bogoliubov rotation angle θ .

The resulting conductance formula is given in Eqs. (3.3)–(3.9) in Sec. III, and its derivation is presented in Sec. V. Further details of the superconducting collision integral, formulated in terms of the Bogoliubov quasiparticles and playing an essential role in the ω^2 and T^2 terms of the vertex corrections, are provided in Appendix B. While the present analysis focuses on the T^2 term of linear conductance, an extension to nonlinear current up to order $(eV)^3$ will be addressed in future work.

We have also examined behavior of the nonlocal conductance over a wide parameter range at zero magnetic field using the numerical renormalization group approach. The Kondo effect dominates the T^2 term of g_{RL} for large U over the region $E_A \lesssim U/2$, corresponding to the area inside the semicircle illustrated in Fig. 2. In contrast, for $E_A \gtrsim U/2$, i.e., outside the semicircle, the Cooper-pair contribution becomes comparable to the Bogoliubov-quasiparticle contribution, particularly for $\pi/3 < \theta < 2\pi/3$, where the coefficient $C_T^{\text{BG}} + 2C_T^{\text{CP}}$ remains positive in the limit $E_A \rightarrow \infty$. This coefficient also exhibits a negative minimum in the crossover region $E_A \simeq U/2$, especially for large U and $\theta \simeq \pi/2$.

In contrast to the T^2 term of nonlocal conductance g_{RL} , the coefficient of the local conductance g_{LL} exhibits a monotonic dependence on E_A , since the Bogoliubov-quasiparticle and Cooper-pair contributions add constructively to g_{LL} . The separate contributions from C_T^{BG} and C_T^{CP} can also be experimentally extracted by measuring the T^2 terms of both g_{RL} and g_{LL} .

ACKNOWLEDGMENTS

We would like to thank Yoichi Tanaka and Yasuhiro Yamada for valuable discussions. This work was supported by JSPS KAKENHI Grant No. JP23K03284.

Appendix A: Fermi liquid theory for equilibrium Bogoliubov quasiparticles

Here, we provide a brief overview of the recent developments in the Fermi liquid theory for the Anderson impurity model, which we apply in this paper to interacting Bogoliubov quasiparticles.

The Fermi liquid properties of Bogoliubov quasiparticles, described by the effective Hamiltonian \mathcal{H}_{eff} of Eq. (2.14), reflect the low-energy asymptotic form of the retarded Green's function,

$$G_{\gamma,\sigma}^r(\omega) = \frac{1}{\omega - E_{A,\sigma} + i\Gamma_N - \Sigma_{\gamma,\sigma}^r(\omega)}. \quad (\text{A1})$$

Fermi-liquid corrections arising from low-lying energy excitations can be systematically obtained by expanding the self-energy $\Sigma_{\gamma,\sigma}^r(\omega)$ around the Fermi energy $\omega = 0$. The phase shift is given by $\delta_\sigma = \cot^{-1} \frac{E_{A,\sigma} + \Sigma_{\gamma,\sigma}^r(0)}{\Gamma_N}$ at $T = eV = 0$. It plays a primary role in the ground-state properties through the Friedel sum rule, $\langle q_{d\sigma} \rangle \xrightarrow{T \rightarrow 0} \delta_\sigma / \pi$ [81]. The spectral weight $\rho_{d\sigma}$ of impurity levels at the Fermi level can also be expressed in the form,

$$\rho_{d\sigma} \equiv -\frac{1}{\pi} \text{Im} G_{\gamma,\sigma}^r(0) \Big|_{T=eV=0} = \frac{\sin^2 \delta_\sigma}{\pi \Gamma_N}. \quad (\text{A2})$$

The leading-order Fermi-liquid corrections are characterized by the wave function renormalization factor z_σ and the linear susceptibilities $\chi_{\sigma\sigma'}$, defined at $T = eV = 0$ with respect to the equilibrium ground state:

$$\frac{1}{z_\sigma} \equiv 1 - \frac{\partial \Sigma_{\gamma,\sigma}^r(\omega)}{\partial \omega} \Big|_{\omega=0}, \quad (\text{A3})$$

$$\chi_{\sigma\sigma'} \equiv -\frac{\partial \langle q_{d\sigma} \rangle}{\partial E_{A,\sigma'}} = \rho_{d\sigma} \tilde{\chi}_{\sigma\sigma'}, \quad (\text{A4})$$

$$\tilde{\chi}_{\sigma\sigma'} \equiv \delta_{\sigma\sigma'} + \frac{\partial \Sigma_{\gamma,\sigma}^r(0)}{\partial E_{A,\sigma'}}. \quad (\text{A5})$$

Yamada and Yosida showed that the renormalization factor z_σ and the diagonal component of $\tilde{\chi}_{\sigma\sigma}$ are related to each other [79], as

$$\frac{1}{z_\sigma} = \tilde{\chi}_{\sigma\sigma}. \quad (\text{A6})$$

Similarly, the off-diagonal susceptibility is related to the causal vertex function $\Gamma_{\sigma\sigma';\sigma'\sigma}^{--;--}(\omega, \omega'; \omega', \omega)$ for Bogoliubov quasiparticles defined with respect to \mathcal{H}_{eff} in Eq. (2.14) at $T = eV = 0$:

$$\chi_{\sigma\sigma'} = -\Gamma_{\sigma\sigma';\sigma'\sigma}^{--;--}(0, 0; 0, 0) \rho_{d\sigma} \rho_{d\sigma'}, \quad \sigma \neq \sigma'. \quad (\text{A7})$$

These relations were derived in the early studies of the Kondo physics from the Ward identity [79–82], which can be expressed in the following form at $T = eV = 0$:

$$\delta_{\sigma\sigma'} \frac{\partial \Sigma_{\gamma,\sigma}^{--}(\omega)}{\partial \omega} + \frac{\partial \Sigma_{\gamma,\sigma}^{--}(\omega)}{\partial E_{A,\sigma'}} = -\Gamma_{\sigma\sigma';\sigma'\sigma}^{--;--}(\omega, 0; 0, \omega) \rho_{d\sigma'}. \quad (\text{A8})$$

The causal self-energy $\Sigma_{\gamma,\sigma}^{--}$ and the retarded self-energy are related at $T = eV = 0$ through

$$\Sigma_{\gamma,\sigma}^{--}(\omega) = \text{Re} \Sigma_{\gamma,\sigma}^r(\omega) + i \text{Im} \Sigma_{\gamma,\sigma}^r(\omega) \text{sgn} \omega. \quad (\text{A9})$$

Physically, Eq. (A8) reflects current conservation around the impurity site [95]. Equations (A6) and (A7) follow from Eq. (A8) and from the property that the diagonal vertex component ($\sigma = \sigma'$) vanishes at zero frequencies ($\omega = \omega' = 0$),

$$\Gamma_{\sigma\sigma;\sigma\sigma}^{--;--}(0, 0; 0, 0) = 0. \quad (\text{A10})$$

It has recently been clarified that the vertex function for $\sigma = \sigma'$ also satisfies the additional property [87, 88],

$$\frac{\partial}{\partial \omega} \text{Re} \Gamma_{\sigma\sigma;\sigma\sigma}^{--;--}(\omega, 0; 0, \omega) \Big|_{\omega \rightarrow 0} = 0. \quad (\text{A11})$$

This implies that the real part of $\Gamma_{\sigma\sigma;\sigma\sigma}^{--;--}(\omega, 0; 0, \omega)$ contains no linear term in ω . As a consequence, the ω^2 term of the real part of the self-energy can be expressed in terms of the derivative of the susceptibility, or equivalently, the three-body correlation function, at $T = eV = 0$ [86–89],

$$\frac{\partial^2}{\partial \omega^2} \text{Re} \Sigma_{\gamma,\sigma}^r(\omega) \Big|_{\omega \rightarrow 0} = \frac{\partial^2 \Sigma_{\gamma,\sigma}^r(0)}{\partial E_{A,\sigma}^2} = \frac{\partial \tilde{\chi}_{\sigma\sigma}}{\partial E_{A,\sigma}}. \quad (\text{A12})$$

Similarly, the coefficient of the T^2 term in $\text{Re} \Sigma_{\gamma,\sigma}^r(0)$ can also be derived from these properties of the vertex function [88].

Consequently, the low-energy asymptotic form of $\Sigma_{\gamma,\sigma}^r(\omega)$ can be exactly determined exactly up to order ω^2 and T^2 :

$$\text{Im} \Sigma_{\gamma,\sigma}^r(\omega) = -\frac{\pi}{2\rho_{d\sigma}} \chi_{\uparrow\downarrow}^2 \left[\omega^2 + (\pi T)^2 \right], \quad (\text{A13})$$

$$\begin{aligned} E_{A,\sigma} + \text{Re} \Sigma_{\gamma,\sigma}^r(\omega) &= \Gamma_N \cot \delta_\sigma + \left(1 - \frac{\chi_{\sigma\sigma}}{\rho_{d\sigma}} \right) \omega \\ &+ \frac{1}{2} \left(\chi_{\sigma\sigma\sigma}^{[3]} + 2\pi \cot \delta_\sigma \chi_{\sigma\sigma}^2 \right) \omega^2 + \frac{1}{6\rho_{d\sigma}} \chi_{\sigma\sigma\sigma}^{[3]} (\pi T)^2. \end{aligned} \quad (\text{A14})$$

Appendix B: Low-energy behavior of $\Pi_U^{j;(s)}$: derivation of Eq. (5.62)

In Sec. VF, we discussed the result for the order- T^2 contribution to the linear-response current $I_{j,\sigma}^{(U)}$ for $j = L, R$, given by Eq. (5.64),, which arises from the first derivative of the interacting self-energy part $\Pi_U^{j;(s)}(\omega)$ with respect to eV . This Appendix is devoted to a detailed derivation of Eq. (5.62).

The function $\Pi_U^{j;(s)}$, defined in Eq. (5.45), is purely imaginary and consists of the lesser $\Sigma_U^{-(s)}(\omega)$ and the greater $\Sigma_U^{+(s)}(\omega)$ self-energies, together with the distribution functions $f_j^{(s)}$ for electrons ($s = e$) and holes ($s = h$). We start with second-order perturbation theory with respect to H_d^U and show how these self-energy components capture the ω^2 and T^2 terms through the superconducting collision integrals of Bogoliubov quasiparticles. We

then take into account the Fermi-liquid corrections arising from multiple scattering processes of the Bogoliubov quasiparticles.

1. Lesser and greater self-energies for nonequilibrium Bogoliubov quasiparticles

The unperturbed retarded Green's function \mathbf{G}_0^r for the impurity site, derived from Eq. (5.25), can be diagonalized via the Bogoliubov transformation as follows:

$$\tilde{\mathbf{G}}_0^r(\omega) \equiv \mathbf{U}^\dagger \mathbf{G}_0^r(\omega) \mathbf{U} = \begin{pmatrix} \tilde{G}_{0;1}^r(\omega) & 0 \\ 0 & \tilde{G}_{0;2}^r(\omega) \end{pmatrix}, \quad (\text{B1})$$

$$\tilde{G}_{0;1}^r(\omega) = \frac{1}{\omega - E_{A,\uparrow} + i\Gamma_N}, \quad (\text{B2})$$

$$\tilde{G}_{0;2}^r(\omega) = \frac{1}{\omega + E_{A,\downarrow} + i\Gamma_N}. \quad (\text{B3})$$

The complex conjugate $\tilde{G}_{0;\zeta}^a(\omega) = \{\tilde{G}_{0;\zeta}^r(\omega)\}^*$ for $\zeta = 1, 2$ corresponds to the advanced Green's function.

In contrast, the Keldysh Green's functions still retain nonzero off-diagonal elements at finite bias voltages $eV \neq 0$, even after carrying out the Bogoliubov transformation:

$$\tilde{\mathbf{G}}_0^{\nu\nu'} \equiv \mathbf{U}^\dagger \mathbf{G}_0^{\nu\nu'} \mathbf{U} = \begin{pmatrix} \tilde{G}_{0;11}^{\nu\nu'} & \tilde{G}_{0;12}^{\nu\nu'} \\ \tilde{G}_{0;21}^{\nu\nu'} & \tilde{G}_{0;22}^{\nu\nu'} \end{pmatrix}. \quad (\text{B4})$$

Specifically, the unperturbed lesser $\tilde{\mathbf{G}}_0^{-+}$ and the greater $\tilde{\mathbf{G}}_0^{+-}$ components can be expressed in the following forms, using Eqs. (5.16) and (5.17) together with Eq. (5.20):

$$\begin{aligned} \tilde{\mathbf{G}}_0^{-+}(\omega) &\equiv -\mathbf{U}^\dagger \mathbf{G}_0^r(\omega) \Sigma_0^{-+}(\omega) \mathbf{G}_0^a(\omega) \mathbf{U} \\ &= 2i\Gamma_N \tilde{\mathbf{G}}_0^r(\omega) \tilde{\mathbf{f}}_{\text{eff}}(\omega) \tilde{\mathbf{G}}_0^a(\omega), \end{aligned} \quad (\text{B5})$$

$$\begin{aligned} \tilde{\mathbf{G}}_0^{+-}(\omega) &\equiv -\mathbf{U}^\dagger \mathbf{G}_0^r(\omega) \Sigma_0^{+-}(\omega) \mathbf{G}_0^a(\omega) \mathbf{U} \\ &= -2i\Gamma_N \tilde{\mathbf{G}}_0^r(\omega) \left[\mathbf{1} - \tilde{\mathbf{f}}_{\text{eff}}(\omega) \right] \tilde{\mathbf{G}}_0^a(\omega). \end{aligned} \quad (\text{B6})$$

Here, $\tilde{\mathbf{f}}_{\text{eff}}(\omega) \equiv \mathbf{U}^\dagger \mathbf{f}_{\text{eff}}(\omega) \mathbf{U}$ represents the effective distribution function, which takes the following form:

$$\begin{aligned} \tilde{\mathbf{f}}_{\text{eff}} &= \frac{f_{\text{eff}}^{(e)} + f_{\text{eff}}^{(h)}}{2} \mathbf{1} + \frac{f_{\text{eff}}^{(e)} - f_{\text{eff}}^{(h)}}{2} \left(\cos \theta \boldsymbol{\tau}_3 - \sin \theta \boldsymbol{\tau}_1 \right) \\ &\xrightarrow{eV \rightarrow 0} f(\omega) \mathbf{1}. \end{aligned} \quad (\text{B7})$$

The unperturbed lesser and greater Green's functions depend on the temperature and bias voltage through the distribution functions $f_{\text{eff}}^{(e)}(\omega)$ and $f_{\text{eff}}^{(h)}(\omega)$, as explicitly listed in Tables I and II.

The off-diagonal elements of both $\tilde{\mathbf{G}}_0^{-+}(\omega)$ and $\tilde{\mathbf{G}}_0^{+-}(\omega)$ vanish at $eV = 0$ and exhibit linear dependence

TABLE I. $\tilde{G}_0^{-+}(\omega)$: Noninteracting lesser Green's function.

$\tilde{G}_{0;11}^{-+}(\omega) = i\Gamma_N \tilde{G}_{0;1}^r(\omega) \tilde{G}_{0;1}^a(\omega) \left[(1 + \cos\theta) f_{\text{eff}}^{(e)}(\omega) + (1 - \cos\theta) f_{\text{eff}}^{(h)}(\omega) \right]$,
$\tilde{G}_{0;22}^{-+}(\omega) = i\Gamma_N \tilde{G}_{0;2}^r(\omega) \tilde{G}_{0;2}^a(\omega) \left[(1 - \cos\theta) f_{\text{eff}}^{(e)}(\omega) + (1 + \cos\theta) f_{\text{eff}}^{(h)}(\omega) \right]$,
$\tilde{G}_{0;21}^{-+}(\omega) = -i\Gamma_N \tilde{G}_{0;2}^r(\omega) \tilde{G}_{0;1}^a(\omega) \sin\theta \left[f_{\text{eff}}^{(e)}(\omega) - f_{\text{eff}}^{(h)}(\omega) \right]$,
$\tilde{G}_{0;12}^{-+}(\omega) = -i\Gamma_N \tilde{G}_{0;1}^r(\omega) \tilde{G}_{0;2}^a(\omega) \sin\theta \left[f_{\text{eff}}^{(e)}(\omega) - f_{\text{eff}}^{(h)}(\omega) \right]$.

TABLE II. $\tilde{G}_0^{+-}(\omega)$: Noninteracting greater Green's function.

$\tilde{G}_{0;11}^{+-}(\omega) = -i\Gamma_N \tilde{G}_{0;1}^r(\omega) \tilde{G}_{0;1}^a(\omega) \left[(1 + \cos\theta) \left\{ 1 - f_{\text{eff}}^{(e)}(\omega) \right\} + (1 - \cos\theta) \left\{ 1 - f_{\text{eff}}^{(h)}(\omega) \right\} \right]$,
$\tilde{G}_{0;22}^{+-}(\omega) = -i\Gamma_N \tilde{G}_{0;2}^r(\omega) \tilde{G}_{0;2}^a(\omega) \left[(1 - \cos\theta) \left\{ 1 - f_{\text{eff}}^{(e)}(\omega) \right\} + (1 + \cos\theta) \left\{ 1 - f_{\text{eff}}^{(h)}(\omega) \right\} \right]$,
$\tilde{G}_{0;21}^{+-}(\omega) = i\Gamma_N \tilde{G}_{0;2}^r(\omega) \tilde{G}_{0;1}^a(\omega) \sin\theta \left[\left\{ 1 - f_{\text{eff}}^{(e)}(\omega) \right\} - \left\{ 1 - f_{\text{eff}}^{(h)}(\omega) \right\} \right]$,
$\tilde{G}_{0;12}^{+-}(\omega) = i\Gamma_N \tilde{G}_{0;1}^r(\omega) \tilde{G}_{0;2}^a(\omega) \sin\theta \left[\left\{ 1 - f_{\text{eff}}^{(e)}(\omega) \right\} - \left\{ 1 - f_{\text{eff}}^{(h)}(\omega) \right\} \right]$.

on eV , with the coefficient given by

$$\frac{\partial}{\partial eV_j} \left[f_{\text{eff}}^{(e)}(\omega) - f_{\text{eff}}^{(h)}(\omega) \right] \Big|_{eV=0} = \frac{2\Gamma_j}{\Gamma_N} \left(-\frac{\partial f(\omega)}{\partial \omega} \right). \quad (\text{B8})$$

Furthermore, the off-diagonal elements of the lesser and greater Green's functions vanish in the limit $\sin\theta = 0$, i.e., when the superconducting proximity effect induced by Γ_S is absent.

Next, in order to clarify the low-energy behavior of $\Pi_U^{j;(s)}$, we calculate the interacting lesser Σ_U^{-+} and the

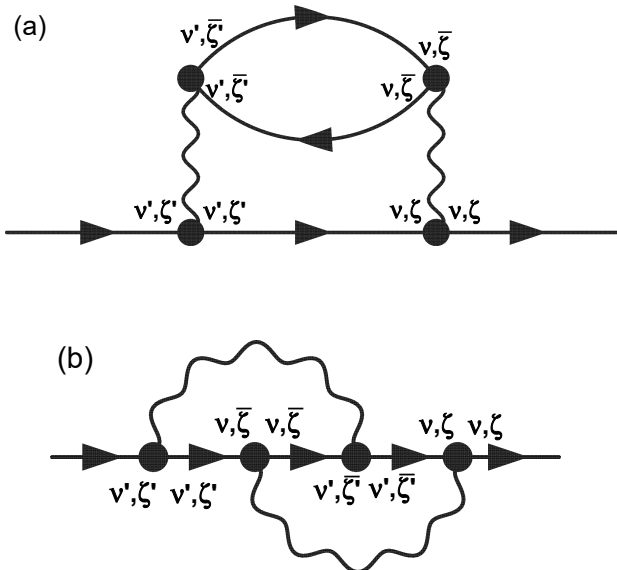


FIG. 11. Feynman diagrams for the order- U^2 self-energy $\tilde{\Sigma}_{U;\zeta\zeta'}^{\nu\nu'}$ of Bogoliubov quasiparticles. The label ζ and its counterpart $\bar{\zeta}$ denote the matrix components in the Nambu pseudo-spin space ($\bar{1} = 2$ and $\bar{2} = 1$), while ν ($= -, +$) labels the Keldysh components.

greater Σ_U^{+-} self-energies by carrying out the Bogoliubov transformation:

$$\tilde{\Sigma}_U^{\nu_4\nu_1} \equiv \mathcal{U}^\dagger \Sigma_U^{\nu_4\nu_1} \mathcal{U}, \quad \tilde{\Pi}_U^{j;(s)} \equiv \mathcal{U}^\dagger \Pi_U^{j;(s)} \mathcal{U}. \quad (\text{B9})$$

The Keldysh perturbation theory with respect to the interacting Hamiltonian H_d^U is naturally formulated at finite bias voltages by using the representation in terms of $\tilde{\psi}_{d,\zeta}$, defined as $\tilde{\psi}_{d,1} \equiv \gamma_{d\uparrow}$ and $\tilde{\psi}_{d,2} \equiv \gamma_{d\downarrow}^\dagger$, introduced in Eq. (5.61). In this basis, the interaction Hamiltonian reads

$$H_d^U \equiv \frac{U}{2} \left(\tilde{\psi}_{d,1}^\dagger \tilde{\psi}_{d,1} - \tilde{\psi}_{d,2}^\dagger \tilde{\psi}_{d,2} \right)^2. \quad (\text{B10})$$

Figure 11 illustrates the Feynman diagrams for the self-energy $\tilde{\Sigma}_{U;\zeta\zeta'}^{\nu\nu'}$ at order U^2 .

Expressions for the lesser $\tilde{\Sigma}_U^{(a)-+}$ and the greater $\tilde{\Sigma}_U^{(a)+-}$ self-energies corresponding to Fig. 11 (a) are listed in Table III for the (1,1) and (2,1) components. The remaining components, namely, $\tilde{\Sigma}_{U;22}^{(a)-+}$, $\tilde{\Sigma}_{U;22}^{(a)+-}$, $\tilde{\Sigma}_{U;12}^{(a)-+}$, and $\tilde{\Sigma}_{U;12}^{(a)+-}$, can be obtained from those listed in the table by interchanging the indices in the subscripts, $1 \Leftrightarrow 2$. For the self-energies $\tilde{\Sigma}_U^{(a)-+}$ and $\tilde{\Sigma}_U^{(a)+-}$, the terms linear in eV arise only from diagonal components, namely $\tilde{\Sigma}_{U;11}^{(a)-+}$, $\tilde{\Sigma}_{U;11}^{(a)+-}$, $\tilde{\Sigma}_{U;22}^{(a)-+}$, and $\tilde{\Sigma}_{U;22}^{(a)+-}$. In contrast, the off-diagonal components, i.e., $\tilde{\Sigma}_{U;21}^{(a)-+}$, $\tilde{\Sigma}_{U;21}^{(a)+-}$, $\tilde{\Sigma}_{U;12}^{(a)-+}$, and $\tilde{\Sigma}_{U;12}^{(a)+-}$, exhibit a $(eV)^3$ dependence at low bias voltages. This behavior originates from the linear dependence on eV of the off-diagonal components of the lesser and greater Green's functions, $\tilde{G}_{0;12}^{-+}(\omega)$, $\tilde{G}_{0;12}^{+-}(\omega)$, $\tilde{G}_{0;21}^{-+}(\omega)$, and $\tilde{G}_{0;21}^{+-}(\omega)$, as discussed above.

Figure 11(b) depicts a second class of order- U^2 scattering processes, which become operative only in the presence of the superconducting proximity effect, i.e., for

TABLE III. Order- U^2 self-energy $\tilde{\Sigma}_U^{(a)\nu\nu'}(\omega)$ corresponding to Fig. 11 (a).

$\tilde{\Sigma}_{U;11}^{(a)-+}(\omega) = -U^2 \int \frac{d\varepsilon_1}{2\pi} \int \frac{d\varepsilon_2}{2\pi} \tilde{G}_{0;22}^{--}(\varepsilon_2) \tilde{G}_{0;22}^{+-}(\varepsilon_1 + \varepsilon_2 - \omega) \tilde{G}_{0;11}^{--}(\varepsilon_1)$,
$\tilde{\Sigma}_{U;11}^{(a)+-}(\omega) = -U^2 \int \frac{d\varepsilon_1}{2\pi} \int \frac{d\varepsilon_2}{2\pi} \tilde{G}_{0;22}^{+-}(\varepsilon_2) \tilde{G}_{0;22}^{--}(\varepsilon_1 + \varepsilon_2 - \omega) \tilde{G}_{0;11}^{+-}(\varepsilon_1)$,
$\tilde{\Sigma}_{U;21}^{(a)-+}(\omega) = -U^2 \int \frac{d\varepsilon_1}{2\pi} \int \frac{d\varepsilon_2}{2\pi} \tilde{G}_{0;12}^{--}(\varepsilon_2) \tilde{G}_{0;12}^{+-}(\varepsilon_1 + \varepsilon_2 - \omega) \tilde{G}_{0;21}^{--}(\varepsilon_1) \xrightarrow{eV \rightarrow 0} O((eV)^3)$,
$\tilde{\Sigma}_{U;21}^{(a)+-}(\omega) = -U^2 \int \frac{d\varepsilon_1}{2\pi} \int \frac{d\varepsilon_2}{2\pi} \tilde{G}_{0;12}^{+-}(\varepsilon_2) \tilde{G}_{0;12}^{--}(\varepsilon_1 + \varepsilon_2 - \omega) \tilde{G}_{0;21}^{+-}(\varepsilon_1) \xrightarrow{eV \rightarrow 0} O((eV)^3)$.

TABLE IV. Order- U^2 self-energy $\tilde{\Sigma}_U^{(b)\nu\nu'}(\omega)$ corresponding to Fig. 11 (b).

$\tilde{\Sigma}_{U;21}^{(b)-+}(\omega) = U^2 \int \frac{d\varepsilon_1}{2\pi} \int \frac{d\varepsilon_2}{2\pi} \tilde{G}_{0;22}^{--}(\varepsilon_2) \tilde{G}_{0;21}^{+-}(\varepsilon_1 + \varepsilon_2 - \omega) \tilde{G}_{0;11}^{--}(\varepsilon_1) \xrightarrow{eV \rightarrow 0} O(eV)$,
$\tilde{\Sigma}_{U;21}^{(b)+-}(\omega) = U^2 \int \frac{d\varepsilon_1}{2\pi} \int \frac{d\varepsilon_2}{2\pi} \tilde{G}_{0;22}^{+-}(\varepsilon_2) \tilde{G}_{0;21}^{--}(\varepsilon_1 + \varepsilon_2 - \omega) \tilde{G}_{0;11}^{+-}(\varepsilon_1) \xrightarrow{eV \rightarrow 0} O(eV)$,
$\tilde{\Sigma}_{U;11}^{(b)-+}(\omega) = U^2 \int \frac{d\varepsilon_1}{2\pi} \int \frac{d\varepsilon_2}{2\pi} \tilde{G}_{0;12}^{--}(\varepsilon_2) \tilde{G}_{0;22}^{+-}(\varepsilon_1 + \varepsilon_2 - \omega) \tilde{G}_{0;21}^{--}(\varepsilon_1) \xrightarrow{eV \rightarrow 0} O((eV)^2)$,
$\tilde{\Sigma}_{U;11}^{(b)+-}(\omega) = U^2 \int \frac{d\varepsilon_1}{2\pi} \int \frac{d\varepsilon_2}{2\pi} \tilde{G}_{0;12}^{+-}(\varepsilon_2) \tilde{G}_{0;22}^{--}(\varepsilon_1 + \varepsilon_2 - \omega) \tilde{G}_{0;21}^{+-}(\varepsilon_1) \xrightarrow{eV \rightarrow 0} O((eV)^2)$.

$\sin \theta \neq 0$. The resulting lesser $\tilde{\Sigma}_U^{(b)-+}$ and greater $\tilde{\Sigma}_U^{(b)+-}$ self-energies are summarized in Table IV for the (1,1) and (2,1) components. All other components, namely, $\tilde{\Sigma}_{U;12}^{(b),-+}$, $\tilde{\Sigma}_{U;12}^{(b),+-}$, $\tilde{\Sigma}_{U;22}^{(b),-+}$, and $\tilde{\Sigma}_{U;22}^{(b),+-}$, follow straightforwardly from those listed by interchanging the indices $1 \Leftrightarrow 2$. At low bias voltages, the off-diagonal (1,2) and (2,1) elements of $\tilde{\Sigma}_U^{(b)-+}$ and $\tilde{\Sigma}_U^{(b)+-}$ exhibit a linear dependence on eV , whereas the diagonal (1,1) and (2,2) elements show a $(eV)^2$ dependence. This behavior originates from the linear dependence on eV of the off-diagonal components of $\tilde{G}_0^{--}(\omega)$ and $\tilde{G}_0^{+-}(\omega)$.

2. Collision integrals for Andreev Scatterings

We next carry out the integrations over ω for the lesser and greater self-energies listed in Tables III and IV in order to clarify the low-energy behavior of $\tilde{\Pi}_U^{j;(s)}$. The low-energy asymptotic forms of these self-energy components are determined by the distribution functions $f_{\text{eff}}^{(e)}$ and $f_{\text{eff}}^{(h)}$, which enter the integrands through the lesser $\tilde{G}_{0;\zeta\zeta'}^{--}$ and the greater $\tilde{G}_{0;\zeta\zeta'}^{+-}$ Green's functions. The contributions arising from these distribution functions can be decomposed into a sum of the superconducting collision integrals $\mathcal{I}_{s's'';s'''}^{+-}$ and $\mathcal{I}_{s's'';s'''}^{+-}$ for $s = e, h$, defined as

$$\mathcal{I}_{s's'';s'''}^{+-}(\omega) \equiv \int_{-\infty}^{\infty} d\varepsilon_1 \int_{-\infty}^{\infty} d\varepsilon_2 \times f_{\text{eff}}^{(s')}(\varepsilon_1) f_{\text{eff}}^{(s'')}(\varepsilon_2) \left[1 - f_{\text{eff}}^{(s''')}(\varepsilon_1 + \varepsilon_2 - \omega) \right], \quad (\text{B11})$$

$$\mathcal{I}_{s's'';s'''}^{+-}(\omega) \equiv \int_{-\infty}^{\infty} d\varepsilon_1 \int_{-\infty}^{\infty} d\varepsilon_2 \times \left[1 - f_{\text{eff}}^{(s')}(\varepsilon_1) \right] \left[1 - f_{\text{eff}}^{(s'')}(\varepsilon_2) \right] f_{\text{eff}}^{(s''')}(\varepsilon_1 + \varepsilon_2 - \omega). \quad (\text{B12})$$

Note that the retarded $\tilde{G}_{0;\zeta}^r(\varepsilon)$ and the advanced $\tilde{G}_{0;\zeta}^a(\varepsilon)$ Green's functions also appear in the integrands together with the distribution functions. However, their frequency dependence does not affect the leading low-energy behavior and can therefore be evaluated at $\varepsilon = 0$.

The lesser collision integral $\mathcal{I}_{s's'';s'''}^{+-}$ has four independent components, since some of the components take identical values owing to the relation $\mu_j^h = -\mu_j^e$:

$$\begin{aligned} \mathcal{I}_{ee;h}^{+-}, \quad & \mathcal{I}_{ee;e}^{+-} = \mathcal{I}_{eh;h}^{+-} = \mathcal{I}_{he;h}^{+-}, \\ \mathcal{I}_{hh;e}^{+-}, \quad & \mathcal{I}_{hh;h}^{+-} = \mathcal{I}_{he;e}^{+-} = \mathcal{I}_{eh;e}^{+-}. \end{aligned} \quad (\text{B13})$$

The same relations also hold for the greater collision integral $\mathcal{I}_{s's'';s'''}^{+-}$. These collision integrals play an essential role in the transport properties of Fermi liquids [69, 70, 95, 105]. They can be evaluated analytically and expressed in the following symmetrized forms:

$$\begin{aligned} \mathcal{I}_{s's'';s'''}^{\text{diff}}(\omega) & \equiv 2 \left[\mathcal{I}_{s's'';s'''}^{+-}(\omega) + \mathcal{I}_{s's'';s'''}^{+-}(\omega) \right] \\ & = \sum_{\substack{j,k,\ell \\ =L,R}} \frac{\Gamma_j \Gamma_k \Gamma_\ell}{(\Gamma_L + \Gamma_R)^3} \left[\left(\omega - \mu_j^{s'} - \mu_k^{s''} + \mu_\ell^{s'''} \right)^2 + (\pi T)^2 \right], \end{aligned} \quad (\text{B14})$$

$$\begin{aligned} \mathcal{I}_{s's'';s'''}^{\text{K}}(\omega) & \equiv 2 \left[\mathcal{I}_{s's'';s'''}^{+-}(\omega) - \mathcal{I}_{s's'';s'''}^{+-}(\omega) \right] \\ & = \sum_{\substack{j,k,\ell \\ =L,R}} \frac{\Gamma_j \Gamma_k \Gamma_\ell}{(\Gamma_L + \Gamma_R)^3} \left[\left(\omega - \mu_j^{s'} - \mu_k^{s''} + \mu_\ell^{s'''} \right)^2 + (\pi T)^2 \right] \\ & \quad \times \left[1 - 2f\left(\omega - \mu_j^{s'} - \mu_k^{s''} + \mu_\ell^{s'''} \right) \right]. \end{aligned} \quad (\text{B15})$$

Table V summarizes the low-energy asymptotic forms of the order- U^2 lesser self-energy components that contribute to the linear conductance. The corresponding

TABLE V. Low-energy asymptotic form of the order- U^2 lesser self-energy $\tilde{\Sigma}_U^{-+}(\omega)$ contributing to the linear conductance. The corresponding greater self-energy $\tilde{\Sigma}_U^{+-}(\omega)$ is obtained from the lesser component by replacing $\mathcal{I}_{s's'';s'''}^{-+}(\omega)$ with $\mathcal{I}_{s's'';s'''}^{+-}(\omega)$ and multiplying by an overall factor of -1 .

$\tilde{\Sigma}_{U;11}^{(a)-+}(\omega)$
$\simeq -i\Gamma_N^3 \tilde{G}_{0;1}^r(0) ^2 \tilde{G}_{0;2}^r(0) ^4 \frac{U^2}{(2\pi)^2} \left[(1 + \cos\theta)^3 \mathcal{I}_{eh;h}^{-+}(\omega) + (1 - \cos\theta)^3 \mathcal{I}_{he;e}^{-+}(\omega) \right.$
$+ (1 + \cos\theta)(1 - \cos\theta)^2 \left\{ \mathcal{I}_{ee;e}^{-+}(\omega) + \mathcal{I}_{he;h}^{-+}(\omega) + \mathcal{I}_{hh;e}^{-+}(\omega) \right\} + (1 + \cos\theta)^2 (1 - \cos\theta) \left\{ \mathcal{I}_{hh;h}^{-+}(\omega) + \mathcal{I}_{eh;e}^{-+}(\omega) + \mathcal{I}_{ee;h}^{-+}(\omega) \right\} \left. \right],$
$\tilde{\Sigma}_{U;22}^{(a)-+}(\omega)$
$\simeq -i\Gamma_N^3 \tilde{G}_{0;1}^r(0) ^4 \tilde{G}_{0;2}^r(0) ^2 \frac{U^2}{(2\pi)^2} \left[(1 + \cos\theta)^3 \mathcal{I}_{he;e}^{-+}(\omega) + (1 - \cos\theta)^3 \mathcal{I}_{eh;h}^{-+}(\omega) \right.$
$+ (1 + \cos\theta)(1 - \cos\theta)^2 \left\{ \mathcal{I}_{hh;h}^{-+}(\omega) + \mathcal{I}_{eh;e}^{-+}(\omega) + \mathcal{I}_{ee;h}^{-+}(\omega) \right\} + (1 + \cos\theta)^2 (1 - \cos\theta) \left\{ \mathcal{I}_{ee;e}^{-+}(\omega) + \mathcal{I}_{he;h}^{-+}(\omega) + \mathcal{I}_{hh;e}^{-+}(\omega) \right\} \left. \right],$
$\tilde{\Sigma}_{U;21}^{(b)-+}(\omega)$
$\simeq -i\Gamma_N^3 \tilde{G}_{0;1}^r(0) ^2 \tilde{G}_{0;2}^r(0) ^2 \tilde{G}_{0;2}^r(0) \tilde{G}_{0;1}^a(0) \frac{U^2}{(2\pi)^2} \sin\theta \left[\sin^2\theta \left\{ \mathcal{I}_{ee;e}^{-+}(\omega) - \mathcal{I}_{hh;h}^{+-}(\omega) + \mathcal{I}_{hh;e}^{-+}(\omega) - \mathcal{I}_{ee;h}^{-+}(\omega) \right\} \right.$
$+ (1 + \cos\theta)^2 \left\{ \mathcal{I}_{eh;e}^{-+}(\omega) - \mathcal{I}_{eh;h}^{-+}(\omega) \right\} + (1 - \cos\theta)^2 \left\{ \mathcal{I}_{he;e}^{-+}(\omega) - \mathcal{I}_{he;h}^{-+}(\omega) \right\} \left. \right],$
$\tilde{\Sigma}_{U;12}^{(b)-+}(\omega)$
$\simeq -i\Gamma_N^3 \tilde{G}_{0;1}^r(0) ^2 \tilde{G}_{0;2}^r(0) ^2 \tilde{G}_{0;1}^r(0) \tilde{G}_{0;2}^a(0) \frac{U^2}{(2\pi)^2} \sin\theta \left[\sin^2\theta \left\{ \mathcal{I}_{ee;e}^{-+}(\omega) - \mathcal{I}_{hh;h}^{+-}(\omega) + \mathcal{I}_{hh;e}^{-+}(\omega) - \mathcal{I}_{ee;h}^{-+}(\omega) \right\} \right.$
$+ (1 + \cos\theta)^2 \left\{ \mathcal{I}_{eh;e}^{-+}(\omega) - \mathcal{I}_{eh;h}^{-+}(\omega) \right\} + (1 - \cos\theta)^2 \left\{ \mathcal{I}_{he;e}^{-+}(\omega) - \mathcal{I}_{he;h}^{-+}(\omega) \right\} \left. \right].$

TABLE VI. Low-energy asymptotic form of the order- U^2 self-energy $\tilde{\Pi}_U^{j;(s)}(\omega)$ with $s = e, h$ contributing to the linear conductance. The prefactor is defined as $\mathcal{A} \equiv \Gamma_N^3 |\tilde{G}_{0;1}^r(0)|^2 |\tilde{G}_{0;2}^r(0)|^2 \frac{U^2}{(2\pi)^2}$.

$\tilde{\Pi}_{U;11}^{(a)j;(s)}(\omega) \simeq -i \frac{\mathcal{A}}{2} \tilde{G}_{0;2}^r(0) ^2 \left[(1 + \cos\theta)^3 \mathcal{I}_{ee;e}^{j;(s)}(\omega) + (1 - \cos\theta)^3 \mathcal{I}_{hh;h}^{j;(s)}(\omega) \right.$
$+ (1 + \cos\theta)(1 - \cos\theta)^2 \left\{ 2\mathcal{I}_{ee;e}^{j;(s)}(\omega) + \mathcal{I}_{hh;e}^{j;(s)}(\omega) \right\} + (1 + \cos\theta)^2 (1 - \cos\theta) \left\{ 2\mathcal{I}_{hh;h}^{j;(s)}(\omega) + \mathcal{I}_{ee;h}^{j;(s)}(\omega) \right\} \left. \right],$
$\tilde{\Pi}_{U;22}^{(a)j;(s)}(\omega) \simeq -i \frac{\mathcal{A}}{2} \tilde{G}_{0;1}^r(0) ^2 \left[(1 + \cos\theta)^3 \mathcal{I}_{hh;h}^{j;(s)}(\omega) + (1 - \cos\theta)^3 \mathcal{I}_{ee;e}^{j;(s)}(\omega) \right.$
$+ (1 + \cos\theta)(1 - \cos\theta)^2 \left\{ 2\mathcal{I}_{hh;h}^{j;(s)}(\omega) + \mathcal{I}_{ee;h}^{j;(s)}(\omega) \right\} + (1 + \cos\theta)^2 (1 - \cos\theta) \left\{ 2\mathcal{I}_{ee;e}^{j;(s)}(\omega) + \mathcal{I}_{hh;e}^{j;(s)}(\omega) \right\} \left. \right],$
$\tilde{\Pi}_{U;21}^{(b)j;(s)}(\omega) \simeq -i \frac{\mathcal{A}}{2} \tilde{G}_{0;2}^r(0) \tilde{G}_{0;1}^a(0) \sin\theta \left[\sin^2\theta \left\{ \mathcal{I}_{ee;e}^{j;(s)}(\omega) - \mathcal{I}_{hh;h}^{j;(s)}(\omega) + \mathcal{I}_{hh;e}^{j;(s)}(\omega) - \mathcal{I}_{ee;h}^{j;(s)}(\omega) \right\} \right.$
$+ (1 + \cos\theta)^2 \left\{ \mathcal{I}_{hh;h}^{j;(s)}(\omega) - \mathcal{I}_{ee;e}^{j;(s)}(\omega) \right\} + (1 - \cos\theta)^2 \left\{ \mathcal{I}_{hh;h}^{j;(s)}(\omega) - \mathcal{I}_{ee;e}^{j;(s)}(\omega) \right\} \left. \right],$
$\tilde{\Pi}_{U;12}^{(b)j;(s)}(\omega) \simeq -i \frac{\mathcal{A}}{2} \tilde{G}_{0;1}^r(0) \tilde{G}_{0;2}^a(0) \sin\theta \left[\sin^2\theta \left\{ \mathcal{I}_{ee;e}^{j;(s)}(\omega) - \mathcal{I}_{hh;h}^{j;(s)}(\omega) + \mathcal{I}_{hh;e}^{j;(s)}(\omega) - \mathcal{I}_{ee;h}^{j;(s)}(\omega) \right\} \right.$
$+ (1 + \cos\theta)^2 \left\{ \mathcal{I}_{hh;h}^{j;(s)}(\omega) - \mathcal{I}_{ee;e}^{j;(s)}(\omega) \right\} + (1 - \cos\theta)^2 \left\{ \mathcal{I}_{hh;h}^{j;(s)}(\omega) - \mathcal{I}_{ee;e}^{j;(s)}(\omega) \right\} \left. \right].$

greater self-energy components can be obtained from the results listed in this table by replacing $\mathcal{I}_{s's'';s'''}^{-+}(\omega)$ with $\mathcal{I}_{s's'';s'''}^{+-}(\omega)$ and multiplying by a factor of -1 . These lesser and greater self-energies contribute to the partial current $I_{j,\sigma}^{(U)}$ via Eqs. (5.44) and (5.45). Table VI summarizes the order U^2 -results for $\tilde{\Pi}_U^{j;(s)}$ in terms of the collision integrals $\mathcal{I}_{s's'';s'''}^{j;(s)}(\omega)$, which are rearranged for

the current expectation values as

$$\mathcal{I}_{s's'';s'''}^{j;(s)}(\omega) \equiv \mathcal{I}_{s's'';s'''}^K(\omega) - \left[1 - 2f_j^{(s)}(\omega) \right] \mathcal{I}_{s's'';s'''}^{\text{diff}}(\omega). \quad (\text{B16})$$

In particular, the part linear in eV of these collision in-

integrals exhibits the ω^2 and T^2 dependences of the form

$$\mathcal{F}(\omega) \equiv 2 \left[\omega^2 + (\pi T)^2 \right] \left(-\frac{\partial f(\omega)}{\partial \omega} \right), \quad (\text{B17})$$

and, more precisely,

$$\frac{\partial}{\partial eV_j} \mathcal{I}_{ee;e}^{j'(s)}(\omega) \Big|_{eV=0} = \left(\eta^{(s)} \delta_{jj'} - \frac{\Gamma_j}{\Gamma_N} \right) \mathcal{F}(\omega), \quad (\text{B18})$$

$$\frac{\partial}{\partial eV_j} \mathcal{I}_{hh;h}^{j'(s)}(\omega) \Big|_{eV=0} = \left(\eta^{(s)} \delta_{jj'} + \frac{\Gamma_j}{\Gamma_N} \right) \mathcal{F}(\omega), \quad (\text{B19})$$

$$\frac{\partial}{\partial eV_j} \mathcal{I}_{ee;h}^{j'(s)}(\omega) \Big|_{eV=0} = \left(\eta^{(s)} \delta_{jj'} - \frac{3\Gamma_j}{\Gamma_N} \right) \mathcal{F}(\omega), \quad (\text{B20})$$

$$\frac{\partial}{\partial eV_j} \mathcal{I}_{hh;e}^{j'(s)}(\omega) \Big|_{eV=0} = \left(\eta^{(s)} \delta_{jj'} + \frac{3\Gamma_j}{\Gamma_N} \right) \mathcal{F}(\omega), \quad (\text{B21})$$

where $\eta^{(e)} = 1$ and $\eta^{(h)} = -1$.

3. Renormalization for $\tilde{\Pi}_U^{j;(s)}$

The low-energy asymptotic form of the lesser self-energy, $\tilde{\Sigma}_U^{-+}$, is determined by the many-body multiple-scattering processes shown in Fig. 10. In these diagrams, the solid lines represent matrix elements of the full interacting Green's function of the Bogoliubov quasiparticles, $\tilde{G}^{\nu\nu'} \equiv \mathcal{U}^\dagger \mathbf{G}_{dd}^{\nu\nu'} \mathcal{U}$. The shaded squares represent the full vertex corrections with respect to H_d^U in Eq. (B10), defined at $\omega = T = eV = 0$. Specifically, the vertex labeled $(--;--)$ denotes the causal component and the one labeled $(++;++)$ is its anti-causal counterpart. These vertices satisfy the following relations: $\tilde{\Gamma}_{21;12}^{--;--}(0, 0; 0, 0) = \tilde{\Gamma}_{12;21}^{--;--}(0, 0; 0, 0)$ and $\tilde{\Gamma}_{12;21}^{++;++}(0, 0; 0, 0) = -\tilde{\Gamma}_{12;21}^{--;--}(0, 0; 0, 0)$. The (1,1) and (2,1) components of $\tilde{\Sigma}_U^{-+}$ can be calculated exactly, up to terms of order ω^2 and T^2 , in the linear-response regime with respect to eV :

$$\begin{aligned} \tilde{\Sigma}_{U;11}^{-+}(\omega) &= \int \frac{d\varepsilon_1}{2\pi} \int \frac{d\varepsilon_2}{2\pi} \tilde{\Gamma}_{21;12}^{--;--}(0, 0; 0, 0) \tilde{\Gamma}_{12;21}^{++;++}(0, 0; 0, 0) \tilde{G}_{22}^{-+}(\varepsilon_2) \tilde{G}_{22}^{+-}(\varepsilon_1 + \varepsilon_2 - \omega) \tilde{G}_{11}^{-+}(\varepsilon_1) + \dots \\ &= -i \frac{2\Gamma_N^3}{\pi^2} \left| \tilde{\Gamma}_{12;21}^{--;--}(0, 0; 0, 0) \right|^2 \left| \tilde{G}_1^r(0) \right|^2 \left| \tilde{G}_2^r(0) \right|^4 \int d\varepsilon_1 \int d\varepsilon_2 \left\{ \tilde{f}_{\text{eff}}(\varepsilon_1) \right\}_{11} \left\{ \tilde{f}_{\text{eff}}(\varepsilon_2) \right\}_{22} \left\{ \mathbf{1} - \tilde{f}_{\text{eff}}(\varepsilon_1 + \varepsilon_2 - \omega) \right\}_{22}, \end{aligned} \quad (\text{B22})$$

$$\begin{aligned} \tilde{\Sigma}_{U;21}^{-+}(\omega) &= - \int \frac{d\varepsilon_1}{2\pi} \int \frac{d\varepsilon_2}{2\pi} \tilde{\Gamma}_{21;12}^{--;--}(0, 0; 0, 0) \tilde{\Gamma}_{12;21}^{++;++}(0, 0; 0, 0) \tilde{G}_{22}^{-+}(\varepsilon_2) \tilde{G}_{21}^{+-}(\varepsilon_1 + \varepsilon_2 - \omega) \tilde{G}_{11}^{-+}(\varepsilon_1) + \dots \\ &= i \frac{2\Gamma_N^3}{\pi^2} \left| \tilde{\Gamma}_{12;21}^{--;--}(0, 0; 0, 0) \right|^2 \left| \tilde{G}_1^r(0) \right|^2 \left| \tilde{G}_2^r(0) \right|^2 \tilde{G}_2^r(0) \tilde{G}_1^a(0) \int d\varepsilon_1 \int d\varepsilon_2 \left\{ \tilde{f}_{\text{eff}}(\varepsilon_1) \right\}_{11} \left\{ \tilde{f}_{\text{eff}}(\varepsilon_2) \right\}_{22} \left\{ \mathbf{1} - \tilde{f}_{\text{eff}}(\varepsilon_1 + \varepsilon_2 - \omega) \right\}_{21}. \end{aligned} \quad (\text{B23})$$

In order to determine the low-energy expansion up to order ω^2 and T^2 , the lesser and greater Green's functions appearing in the integrands of the first lines of Eqs. (B22) and (B23), have been replaced by

$$\begin{aligned} \tilde{G}^{-+}(\omega) &\equiv -\tilde{G}^r(\omega) \left[\tilde{\Sigma}_0^{-+}(\omega) + \tilde{\Sigma}_U^{-+}(\omega) \right] \tilde{G}^a(\omega) \\ &= 2i\Gamma_N \tilde{G}^r(0) \tilde{f}_{\text{eff}}(\omega) \tilde{G}^a(0) + \dots, \end{aligned} \quad (\text{B24})$$

$$\begin{aligned} \tilde{G}^{+-}(\omega) &\equiv -\tilde{G}^r(\omega) \left[\tilde{\Sigma}_0^{+-}(\omega) + \tilde{\Sigma}_U^{+-}(\omega) \right] \tilde{G}^a(\omega) \\ &= -2i\Gamma_N \tilde{G}^r(0) \left[\mathbf{1} - \tilde{f}_{\text{eff}}(\omega) \right] \tilde{G}^a(0) + \dots. \end{aligned} \quad (\text{B25})$$

This is because the contributions from $\tilde{\Sigma}_U^{-+}$ and $\tilde{\Sigma}_U^{+-}$ terms, which enter through the internal lines of these Feynman diagrams, ultimately generate terms beyond order T^2 in the current. The integrals involving the distribution functions \tilde{f}_{eff} in the last lines of Eqs. (B22) and (B23) can therefore be expressed in terms of the collision integrals $\mathcal{I}_{s's'';s'''}^{-+}$ defined in Sec. B 2.

These low-energy asymptotic forms of $\tilde{\Sigma}_{U;11}^{-+}(\omega)$ and $\tilde{\Sigma}_{U;21}^{-+}(\omega)$ can be compared with the corresponding perturbative results shown in Table V. The perturbative results capture the essential functional structure of the asymptotic forms, and they become identical to the exact ones upon replacing the bare interaction strength U^2 with $\left| \tilde{\Gamma}_{12;21}^{--;--}(0, 0; 0, 0) \right|^2$, the full scattering strength determined by the vertex function, and further substituting the noninteracting Green's functions $\tilde{G}_{0;\zeta}^r(0)$ and $\tilde{G}_{0;\zeta}^a(0)$ with the corresponding full Green's functions $\tilde{G}_\zeta^r(0)$ and $\tilde{G}_\zeta^a(0)$, respectively. The other components of the lesser self-energy, $\tilde{\Sigma}_{U;22}^{-+}$ and $\tilde{\Sigma}_{U;12}^{-+}$, can also be obtained from Eqs. (B22) and (B23) by interchanging the indices $1 \leftrightarrow 2$. Furthermore, the low-energy asymptotic form of greater self-energy $\tilde{\Sigma}_U^{+-}$ can be obtained in a similar manner by exchanging $- \leftrightarrow +$ and then using Eqs. (B24) and (B25). The low-energy asymptotic forms of all these lesser and greater self-energies exhibit the same functional structure as the perturbative results, differing only in the over-

all coefficients renormalized by multiple scattering processes.

Similarly, the exact low-energy asymptotic form of $\tilde{\Pi}_U^{j';(s)}$ can be derived from the corresponding perturbative results summarized in Table VI, by replacing the

$$\begin{aligned} \frac{\partial \tilde{\Pi}_U^{j';(s)}}{\partial eV_j} \Big|_{eV=0} &= -2i \frac{\Gamma_N^3}{\pi^2} |\tilde{G}_1^r(0)|^2 |\tilde{G}_2^r(0)|^2 \left| \tilde{\Gamma}_{12;21}^{--;--}(0,0;0,0) \right|^2 \left[\omega^2 + (\pi T)^2 \right] \left(-\frac{\partial f(\omega)}{\partial \omega} \right) \\ &\times \left\{ \eta^{(s)} \delta_{jj'} \begin{pmatrix} |\tilde{G}_2^r(0)|^2 & 0 \\ 0 & |\tilde{G}_1^r(0)|^2 \end{pmatrix} - \frac{\Gamma_j}{\Gamma_N} \cos \theta \begin{pmatrix} |\tilde{G}_2^r(0)|^2 & 0 \\ 0 & -|\tilde{G}_1^r(0)|^2 \end{pmatrix} + \frac{\Gamma_j}{\Gamma_N} \sin \theta \begin{pmatrix} 0 & \tilde{G}_1^r(0) \tilde{G}_2^a(0) \\ \tilde{G}_2^r(0) \tilde{G}_1^a(0) & 0 \end{pmatrix} \right\}, \end{aligned} \quad (\text{B26})$$

where $\eta^{(e)} = 1$ and $\eta^{(h)} = -1$.

In order to derive the linear-response contribution to $I_{j,\sigma}^{(U)}$ using Eqs. (5.39) and (5.40), we next evaluate the diagonal elements of the matrix product, $\mathbf{G}_{dd}^r(0) \frac{\partial \tilde{\Pi}_U^{j';(s)}}{\partial eV_j} \mathbf{G}_{dd}^a(0)$. Carrying out the inverse Bogoliubov transformation for the three matrices appearing on the right-hand side of Eq. (B26), the matrices in the first and second terms can be expressed in the following forms:

$$\begin{aligned} \mathbf{G}_{dd}^r(0) \mathbf{U} \begin{pmatrix} |\tilde{G}_2^r(0)|^2 & 0 \\ 0 & |\tilde{G}_1^r(0)|^2 \end{pmatrix} \mathbf{U}^\dagger \mathbf{G}_{dd}^a(0) \\ = |\tilde{G}_1^r(0)|^2 |\tilde{G}_2^r(0)|^2 \mathbf{1}, \end{aligned} \quad (\text{B27})$$

and

$$\begin{aligned} \mathbf{G}_{dd}^r(0) \mathbf{U} \begin{pmatrix} |\tilde{G}_2^r(0)|^2 & 0 \\ 0 & -|\tilde{G}_1^r(0)|^2 \end{pmatrix} \mathbf{U}^\dagger \mathbf{G}_{dd}^a(0) \\ = |\tilde{G}_1^r(0)|^2 |\tilde{G}_2^r(0)|^2 (\cos \theta \boldsymbol{\tau}_3 + \sin \theta \boldsymbol{\tau}_1), \end{aligned} \quad (\text{B28})$$

The third term is transformed into the following form:

$$\begin{aligned} \mathbf{G}_{dd}^r(0) \mathbf{U} \begin{pmatrix} 0 & \tilde{G}_1^r(0) \tilde{G}_2^a(0) \\ \tilde{G}_2^r(0) \tilde{G}_1^a(0) & 0 \end{pmatrix} \mathbf{U}^\dagger \mathbf{G}_{dd}^a(0) \\ = \mathbf{U} \begin{pmatrix} 0 & \left\{ \tilde{G}_1^r(0) \tilde{G}_2^a(0) \right\}^2 \\ \left\{ \tilde{G}_2^r(0) \tilde{G}_1^a(0) \right\}^2 & 0 \end{pmatrix} \mathbf{U}^\dagger \\ = -\frac{\left\{ \tilde{G}_1^r(0) \tilde{G}_2^a(0) \right\}^2 + \left\{ \tilde{G}_2^r(0) \tilde{G}_1^a(0) \right\}^2}{2} \sin \theta \boldsymbol{\tau}_3 \\ + \text{(off-diagonal matrix components)}. \end{aligned} \quad (\text{B29})$$

bare parameters with their renormalized counterparts, $U^2 \Rightarrow \left| \tilde{\Gamma}_{12;21}^{--;--}(0,0;0,0) \right|^2$, and $\tilde{G}_{0;\zeta}^{r/a}(0) \Rightarrow \tilde{G}_\zeta^{r/a}(0)$. Thus, the first derivative of $\tilde{\Pi}_U^{j';(s)}$ with respect to eV can be expressed in the following form, using also Eqs. (B18)–(B21):

Thus, the diagonal elements of $\mathbf{G}_{dd}^r(0) \frac{\partial \tilde{\Pi}_U^{j';(s)}}{\partial eV_j} \mathbf{G}_{dd}^a(0)$ consist of a linear combination of $\eta^{(s)} \mathbf{1}$ and $\boldsymbol{\tau}_3$. Consequently, the (1,1) element of the matrix for $s = e$ and the (2,2) element of one for $s = h$ are equal in magnitude but opposite in sign:

$$\begin{aligned} &- \left\{ \mathbf{G}_{dd}^r(0) \frac{\partial \tilde{\Pi}_U^{j';(h)}}{\partial eV_j} \Big|_{eV=0} \mathbf{G}_{dd}^a(0) \right\}_{22} \\ &= \left\{ \mathbf{G}_{dd}^r(0) \frac{\partial \tilde{\Pi}_U^{j';(e)}}{\partial eV_j} \Big|_{eV=0} \mathbf{G}_{dd}^a(0) \right\}_{11}. \end{aligned} \quad (\text{B30})$$

This implies that $I_{j,\uparrow}^{(U)} = I_{j,\downarrow}^{(U)}$ in the linear-response regime, whereas $I_{j,\sigma}^{(0)}$ generally depends on the spin component σ .

The above discussion mainly employs the Keldysh Green's functions $\tilde{G}_{\zeta\zeta'}^{\nu\nu'}$, defined in terms of the operators $\tilde{\psi}_{d,\zeta}$ with $\zeta = 1, 2$. The coefficients appearing in Eq. (B26) can alternatively be expressed in terms of the Fermi-liquid parameters defined with respect to the operators $\gamma_{d\uparrow} = \tilde{\psi}_{d,1}$ and $\gamma_{d\downarrow} = \tilde{\psi}_{d,2}^\dagger$. The correspondence between the vertex functions in these two representations is given by $\tilde{\Gamma}_{12;21}^{--;--}(0,0;0,0) = -\Gamma_{\uparrow\downarrow;\uparrow\downarrow}^{--;--}(0,0;0,0)$. For the retarded Green's functions, we have $\tilde{G}_1^r(\omega) = G_{\gamma,\uparrow}^r(\omega)$ and $\tilde{G}_2^r(\omega) = -G_{\gamma,\downarrow}^a(-\omega)$. In particular, at $\omega = T = eV = 0$, these Green's functions can be expressed in terms of the phase shifts as follows:

$$G_{\gamma,\sigma}^r(0) = -\frac{e^{i\delta_\sigma} \sin \delta_\sigma}{\Gamma_N}, \quad \rho_{d\sigma} \equiv \frac{\sin^2 \delta_\sigma}{\pi \Gamma_N}. \quad (\text{B31})$$

Therefore,

$$\begin{aligned}
& \frac{\left\{ \tilde{G}_1^r(0)\tilde{G}_2^a(0) \right\}^2 + \left\{ \tilde{G}_2^r(0)\tilde{G}_1^a(0) \right\}^2}{2} \\
&= \frac{\left\{ G_{\gamma,\uparrow}^r(0)G_{\gamma,\downarrow}^r(0) \right\}^2 + \left\{ G_{\gamma,\uparrow}^a(0)G_{\gamma,\downarrow}^a(0) \right\}^2}{2} \\
&= |G_{\gamma,\uparrow}^r(0)|^2 |G_{\gamma,\downarrow}^r(0)|^2 \cos 2(\delta_\uparrow + \delta_\downarrow). \quad (B32)
\end{aligned}$$

Moreover, the vertex function can be expressed in terms of $\chi_{\uparrow\downarrow}$ defined in Eq. (A7) as

$$\begin{aligned}
& \frac{\Gamma_N^2}{\pi^2} |\tilde{G}_1^r(0)|^2 |\tilde{G}_2^r(0)|^2 \tilde{\Gamma}_{12;21}^{--;--}(0, 0; 0, 0) \\
&= -\Gamma_{\uparrow\downarrow;\uparrow}^{--;--}(0, 0; 0, 0) \rho_{d\uparrow} \rho_{d\downarrow} = \chi_{\uparrow\downarrow}. \quad (B33)
\end{aligned}$$

Using these relations together with Eqs. (B27)–(B29), Eq. (B26) can be rewritten in the following form, which is also presented in the main text as Eq. (5.62):

$$\begin{aligned}
& \left\{ \mathbf{G}_{dd}^r(0) \left. \frac{\partial \mathbf{\Pi}_U^{j';(e)}}{\partial eV_j} \right|_{eV=0} \mathbf{G}_{dd}^a(0) \right\}_{11} \\
&= -2i \frac{\Gamma_N^3}{\pi^2} |G_{\gamma,\uparrow}^r(0)|^4 |G_{\gamma,\downarrow}^r(0)|^4 \left| \Gamma_{\uparrow\downarrow;\uparrow}^{--;--}(0, 0; 0, 0) \right|^2 \left[\omega^2 + (\pi T)^2 \right] \left(-\frac{\partial f(\omega)}{\partial \omega} \right) \\
&\quad \times \left[\left(\delta_{jj'} - \frac{\Gamma_j}{\Gamma_N} \cos^2 \theta \right) - \frac{\Gamma_j}{\Gamma_N} \cos 2(\delta_\uparrow + \delta_\downarrow) \sin^2 \theta \right] \\
&= -i \frac{2\pi^2 \chi_{\uparrow\downarrow}^2}{\Gamma_N} \left[\omega^2 + (\pi T)^2 \right] \left(-\frac{\partial f(\omega)}{\partial \omega} \right) \left[\left(\delta_{jj'} - \frac{\Gamma_j}{\Gamma_N} \right) + \frac{\Gamma_j}{\Gamma_N} 2 \sin^2(\delta_\uparrow + \delta_\downarrow) \sin^2 \theta \right]. \quad (B34)
\end{aligned}$$

[1] J. Schindeler, A. Baumgartner, R. Maurand, M. Weiss, and C. Schönenberger, Nonlocal spectroscopy of Andreev bound states, *Phys. Rev. B* **89**, 045422 (2014).

[2] E. J. H. Lee, X. Jiang, M. Houzet, R. Aguado, C. M. Lieber, and S. De Franceschi, Spin-resolved Andreev levels and parity crossings in hybrid superconductor–semiconductor nanostructures, *Nature Nanotechnology* **9**, 79 (2014).

[3] A. Bordoloi, V. Zannier, L. Sorba, C. Schönenberger, and A. Baumgartner, Spin cross-correlation experiments in an electron entangler, *Nature* **612**, 454 (2022).

[4] D. S. Golubev and A. D. Zaikin, Non-local Andreev reflection in superconducting quantum dots, *Phys. Rev. B* **76**, 184510 (2007).

[5] L. Hofstetter, S. Csonka, J. Nygård, and C. Schönenberger, Cooper pair splitter realized in a two-quantum-dot Y-junction, *Nature* **461**, 960 (2009).

[6] J. Schindeler, A. Baumgartner, and C. Schönenberger, Near-Unity Cooper Pair Splitting Efficiency, *Phys. Rev. Lett.* **109**, 157002 (2012).

[7] A. Das, Y. Ronen, M. Heiblum, D. Mahalu, A. V. Kretinin, and H. Shtrikman, High-efficiency Cooper pair splitting demonstrated by two-particle conductance resonance and positive noise cross-correlation, *Nature Communications* **3**, 1165 (2012).

[8] G. Fülop, S. d’Holllosy, A. Baumgartner, P. Makk, V. A. Guzenko, M. H. Madsen, J. Nygård, C. Schönenberger, and S. Csonka, Local electrical tuning of the nonlocal signals in a Cooper pair splitter, *Phys. Rev. B* **90**, 235412 (2014).

[9] Z. B. Tan, D. Cox, T. Nieminen, P. Lähteenmäki, D. Golubev, G. B. Lesovik, and P. J. Hakonen, Cooper Pair Splitting by Means of Graphene Quantum Dots, *Phys. Rev. Lett.* **114**, 096602 (2015).

[10] I. V. Borzenets, Y. Shimazaki, G. F. Jones, M. F. Craciun, S. Russo, M. Yamamoto, and S. Tarucha, High Efficiency CVD Graphene-lead (Pb) Cooper Pair Splitter, *Scientific Reports* **6**, 23051 (2016).

[11] Z. B. Tan, A. Laitinen, N. S. Kirsanov, A. Galda, V. M. Vinokur, M. Haque, A. Savin, D. S. Golubev, G. B. Lesovik, and P. J. Hakonen, Thermoelectric current in a graphene Cooper pair splitter, *Nature Communications* **12**, 138 (2021).

[12] J. Rech, D. Chevallier, T. Jonckheere, and T. Martin, Current correlations in an interacting Cooper-pair beam splitter, *Phys. Rev. B* **85**, 035419 (2012).

[13] R. Sánchez, P. Burset, and A. L. Yeyati, Cooling by Cooper pair splitting, *Phys. Rev. B* **98**, 241414 (2018).

[14] N. S. Kirsanov, Z. B. Tan, D. S. Golubev, P. J. Hakonen, and G. B. Lesovik, Heat switch and thermoelectric effects based on Cooper-pair splitting and elastic cotunneling, *Phys. Rev. B* **99**, 115127 (2019).

[15] N. Walldorf, C. Padurariu, A.-P. Jauho, and C. Flindt, Electron Waiting Times of a Cooper Pair Splitter, *Phys. Rev. Lett.* **120**, 087701 (2018).

[16] R. Hussein, M. Governale, S. Kohler, W. Belzig, F. Giacotto, and A. Braggio, Nonlocal thermoelectricity in a

Cooper-pair splitter, Phys. Rev. B **99**, 075429 (2019).

[17] A. Ranni, F. Brange, E. T. Mannila, C. Flindt, and V. F. Maisi, Real-time observation of Cooper pair splitting showing strong non-local correlations, Nature Communications **12**, 6358 (2021).

[18] A. V. Rozhkov and D. P. Arovas, Josephson Coupling through a Magnetic Impurity, Phys. Rev. Lett. **82**, 2788 (1999).

[19] A. A. Clerk and V. Ambegaokar, Loss of π -junction behavior in an interacting impurity Josephson junction, Phys. Rev. B **61**, 9109 (2000).

[20] E. Vecino, A. Martín-Rodero, and A. L. Yeyati, Josephson current through a correlated quantum level: Andreev states and π junction behavior, Phys. Rev. B **68**, 035105 (2003).

[21] T. Yoshioka and Y. Ohashi, Numerical Renormalization Group Studies on Single Impurity Anderson Model in Superconductivity: A Unified Treatment of Magnetic, Nonmagnetic Impurities, and Resonance Scattering, J. Phys. Soc. Jpn. **69**, 1812 (2000).

[22] M.-S. Choi, M. Lee, K. Kang, and W. Belzig, Kondo effect and Josephson current through a quantum dot between two superconductors, Phys. Rev. B **70**, 020502 (2004).

[23] F. Siano and R. Egger, Josephson Current through a Nanoscale Magnetic Quantum Dot, Phys. Rev. Lett. **93**, 047002 (2004).

[24] A. Oguri, Y. Tanaka, and A. C. Hewson, Quantum Phase Transition in a Minimal Model for the Kondo Effect in a Josephson Junction, J. Phys. Soc. Jpn. **73**, 2494 (2004).

[25] J. Bauer, A. Oguri, and A. C. Hewson, Spectral properties of locally correlated electrons in a Bardeen-Cooper-Schrieffer superconductor, Journal of Physics: Condensed Matter **19**, 486211 (2007).

[26] Y. Tanaka, A. Oguri, and A. C. Hewson, Kondo effect in asymmetric Josephson couplings through a quantum dot, New J. Phys. **9**, 115 (2007).

[27] C. Karrasch, A. Oguri, and V. Meden, Josephson current through a single Anderson impurity coupled to BCS leads, Phys. Rev. B **77**, 024517 (2008).

[28] T. Meng, S. Florens, and P. Simon, Self-consistent description of andreev bound states in josephson quantum dot devices, Phys. Rev. B **79**, 224521 (2009).

[29] T. Hecht, A. Weichselbaum, J. von Delft, and R. Bulla, Numerical renormalization group calculation of near-gap peaks in spectral functions of the Anderson model with superconducting leads, Journal of Physics: Condensed Matter **20**, 275213 (2008).

[30] Y. Tanaka, N. Kawakami, and A. Oguri, Numerical Renormalization Group Approach to a Quantum Dot Coupled to Normal and Superconducting Leads, J. Phys. Soc. Jpn. **76**, 074701 (2007).

[31] Y. Yamada, Y. Tanaka, and N. Kawakami, Interplay of Kondo and superconducting correlations in the nonequilibrium Andreev transport through a quantum dot, Phys. Rev. B **84**, 075484 (2011).

[32] C. Buijzer, A. Oiwa, K. Shibata, K. Hirakawa, and S. Tarucha, Kondo Universal Scaling for a Quantum Dot Coupled to Superconducting Leads, Phys. Rev. Lett. **99**, 136806 (2007).

[33] R. S. Deacon, Y. Yamada, A. Oiwa, R. Sakano, K. Yoshida, K. Shibata, K. Hirakawa, and S. Tarucha, Tunneling Spectroscopy of Andreev Energy Levels in a Quantum Dot Coupled to a Superconductor, Phys. Rev. Lett. **104**, 076805 (2010).

[34] R. S. Deacon, Y. Tanaka, A. Oiwa, R. Sakano, K. Yoshida, K. Shibata, K. Hirakawa, and S. Tarucha, Kondo-enhanced Andreev transport in single self-assembled InAs quantum dots contacted with normal and superconducting leads, Phys. Rev. B **81**, 121308 (2010).

[35] M. Governale, M. G. Pala, and J. König, Real-time diagrammatic approach to transport through interacting quantum dots with normal and superconducting leads, Phys. Rev. B **77**, 134513 (2008).

[36] D. Futterer, M. Governale, M. G. Pala, and J. König, Nonlocal Andreev transport through an interacting quantum dot, Phys. Rev. B **79**, 054505 (2009).

[37] J. Eldridge, M. G. Pala, M. Governale, and J. König, Superconducting proximity effect in interacting double-dot systems, Phys. Rev. B **82**, 184507 (2010).

[38] G. Michalek, B. R. Bulka, T. Domański, and K. I. Wysokiński, Interplay between direct and crossed Andreev reflections in hybrid nanostructures, Phys. Rev. B **88**, 155425 (2013).

[39] A. Oguri, Y. Tanaka, and J. Bauer, Interplay between Kondo and Andreev-Josephson effects in a quantum dot coupled to one normal and two superconducting leads, Phys. Rev. B **87**, 075432 (2013).

[40] A. Koga, Quantum Monte Carlo study of nonequilibrium transport through a quantum dot coupled to normal and superconducting leads, Phys. Rev. B **87**, 115409 (2013).

[41] T. Domański, M. Žonda, V. Pokorný, G. Górska, V. Janiš, and T. Novotný, Josephson-phase-controlled interplay between correlation effects and electron pairing in a three-terminal nanostructure, Phys. Rev. B **95**, 045104 (2017).

[42] K. Wrześniowski and I. Weymann, Kondo physics in double quantum dot based Cooper pair splitters, Phys. Rev. B **96**, 195409 (2017).

[43] M. Lee, R. López, H. Q. Xu, and G. Platero, Proposal for Detection of the $0'$ and π' Phases in Quantum-Dot Josephson Junctions, Phys. Rev. Lett. **129**, 207701 (2022).

[44] J.-D. Pillet, P. Joyez, R. Žitko, and M. F. Goffman, Tunneling spectroscopy of a single quantum dot coupled to a superconductor: From Kondo ridge to Andreev bound states, Phys. Rev. B **88**, 045101 (2013).

[45] A. Kadlecová, M. Žonda, and T. Novotný, Quantum dot attached to superconducting leads: Relation between symmetric and asymmetric coupling, Phys. Rev. B **95**, 195114 (2017).

[46] V. Pokorný and M. Žonda, Effective low-energy models for superconducting impurity systems, Phys. Rev. B **107**, 155111 (2023).

[47] K. P. Wójcik and I. Weymann, Nonlocal pairing as a source of spin exchange and Kondo screening, Phys. Rev. B **99**, 045120 (2019).

[48] N. Walldorf, F. Brange, C. Padurariu, and C. Flindt, Noise and full counting statistics of a Cooper pair splitter, Phys. Rev. B **101**, 205422 (2020).

[49] M. Hashimoto, Y. Yamada, Y. Tanaka, Y. Teratani, T. Kemi, N. Kawakami, and A. Oguri, Nonlocal Andreev transport through a quantum dot in a magnetic field: Interplay between Kondo, Zeeman, and Cooper-

pair correlations, Phys. Rev. B **109**, 035404 (2024).

[50] Y. Tanaka, N. Kawakami, and A. Oguri, Andreev transport through side-coupled double quantum dots, Phys. Rev. B **78**, 035444 (2008).

[51] D. Goldhaber-Gordon, H. Shtrikman, D. Mahalu, D. Abusch-Magder, U. Meirav, and M. A. Kastner, Kondo effect in a single-electron transistor, Nature **391**, 156 (1998).

[52] D. Goldhaber-Gordon, J. Göres, M. A. Kastner, H. Shtrikman, D. Mahalu, and U. Meirav, From the Kondo Regime to the Mixed-Valence Regime in a Single-Electron Transistor, Phys. Rev. Lett. **81**, 5225 (1998).

[53] S. M. Cronenwett, T. H. Oosterkamp, and L. P. Kouwenhoven, A Tunable Kondo Effect in Quantum Dots, Science **281**, 540 (1998).

[54] W. G. van der Wiel, S. D. Franceschi, T. Fujisawa, J. M. Elzerman, S. Tarucha, and L. P. Kouwenhoven, The Kondo Effect in the Unitary Limit, Science **289**, 2105 (2000).

[55] I. V. Borzenets, J. Shim, J. C. H. Chen, A. Ludwig, A. D. Wieck, S. Tarucha, H.-S. Sim, and M. Yamamoto, Observation of the Kondo screening cloud, Nature **579**, 210 (2020).

[56] M. Grobis, I. G. Rau, R. M. Potok, H. Shtrikman, and D. Goldhaber-Gordon, Universal Scaling in Nonequilibrium Transport through a Single Channel Kondo Dot, Phys. Rev. Lett. **100**, 246601 (2008).

[57] G. D. Scott, Z. K. Keane, J. W. Ciszek, J. M. Tour, and D. Natelson, Universal scaling of nonequilibrium transport in the Kondo regime of single molecule devices, Phys. Rev. B **79**, 165413 (2009).

[58] O. Zarchin, M. Zaffalon, M. Heiblum, D. Mahalu, and V. Umansky, Two-electron bunching in transport through a quantum dot induced by Kondo correlations, Phys. Rev. B **77**, 241303(R) (2008).

[59] T. Delattre, C. Feuillet-Palma, L. G. Herrmann, P. Morfin, J.-M. Berroir, G. Fève, B. Plaçais, D. C. Glattli, M.-S. Choi, C. Mora, and T. Kontos, Noisy Kondo impurities, Nat. Phys. **5**, 208 (2009).

[60] Y. Yamauchi, K. Sekiguchi, K. Chida, T. Arakawa, S. Nakamura, K. Kobayashi, T. Ono, T. Fujii, and R. Sakano, Evolution of the Kondo Effect in a Quantum Dot Probed by Shot Noise, Phys. Rev. Lett. **106**, 176601 (2011).

[61] M. Ferrier, T. Arakawa, T. Hata, R. Fujiwara, R. Delagrange, R. Weil, R. Deblock, R. Sakano, A. Oguri, and K. Kobayashi, Universality of non-equilibrium fluctuations in strongly correlated quantum liquids, Nat. Phys. **12**, 230 (2016).

[62] T. Hata, Y. Teratani, T. Arakawa, S. Lee, M. Ferrier, R. Deblock, R. Sakano, A. Oguri, and K. Kobayashi, Three-body correlations in nonlinear response of correlated quantum liquid, Nature Communications **12**, 3233 (2021).

[63] C. Hsu, T. A. Costi, D. Vogel, C. Wegeberg, M. Mayor, H. S. J. van der Zant, and P. Gehring, Magnetic-Field Universality of the Kondo Effect Revealed by Thermocurrent Spectroscopy, Phys. Rev. Lett. **128**, 147701 (2022).

[64] A. Svilans, M. Josefsson, A. M. Burke, S. Fahlvik, C. Thelander, H. Linke, and M. Leijnse, Thermoelectric Characterization of the Kondo Resonance in Nanowire Quantum Dots, Phys. Rev. Lett. **121**, 206801 (2018).

[65] S. Hershfield, J. H. Davies, and J. W. Wilkins, Resonant tunneling through an Anderson impurity. I. Current in the symmetric model, Phys. Rev. B **46**, 7046 (1992).

[66] W. Izumida, O. Sakai, and S. Suzuki, Kondo Effect in Tunneling through a Quantum Dot, J. Phys. Soc. Japan **70**, 1045 (2001).

[67] A. Oguri, Fermi-liquid theory for the Anderson model out of equilibrium, Phys. Rev. B **64**, 153305 (2001).

[68] E. Sela and J. Malecki, Nonequilibrium conductance of asymmetric nanodevices in the Kondo regime, Phys. Rev. B **80**, 233103 (2009).

[69] A. A. Aligia, Nonequilibrium conductance of a nanodevice for small bias voltage, J. Phys.: Condens. Matter **24**, 015306 (2012).

[70] A. A. Aligia, Nonequilibrium self-energies, Ng approach, and heat current of a nanodevice for small bias voltage and temperature, Phys. Rev. B **89**, 125405 (2014).

[71] S. Hershfield, Resonant tunneling through an Anderson impurity. II. Noise in the Hartree approximation, Phys. Rev. B **46**, 7061 (1992).

[72] A. O. Gogolin and A. Komnik, Full Counting Statistics for the Kondo Dot in the Unitary Limit, Phys. Rev. Lett. **97**, 016602 (2006).

[73] E. Sela, Y. Oreg, F. von Oppen, and J. Koch, Fractional Shot Noise in the Kondo Regime, Phys. Rev. Lett. **97**, 086601 (2006).

[74] A. Golub, Shot noise near the unitary limit of a Kondo quantum dot, Phys. Rev. B **73**, 233310 (2006).

[75] A. Oguri, R. Sakano, and T. Fujii, $1/(N-1)$ expansion based on a perturbation theory in U for the Anderson model with N -fold degeneracy, Phys. Rev. B **84**, 113301 (2011).

[76] T. A. Costi and V. Zlatić, Thermoelectric transport through strongly correlated quantum dots, Phys. Rev. B **81**, 235127 (2010).

[77] T. A. Costi, Magnetic field dependence of the thermopower of Kondo-correlated quantum dots: Comparison with experiment, Phys. Rev. B **100**, 155126 (2019).

[78] P. Nozières, A Fermi-liquid description of the Kondo problem at low temperatures, J. Low Temp. Phys. **17**, 31 (1974).

[79] K. Yamada, Perturbation Expansion for the Anderson Hamiltonian. II, Prog. Theor. Phys. **53**, 970 (1975).

[80] K. Yamada, Perturbation Expansion for the Anderson Hamiltonian. IV, Prog. Theor. Phys. **54**, 316 (1975).

[81] H. Shiba, The Korringa Relation for the Impurity Nuclear Spin-Lattice Relaxation in Dilute Kondo Alloys, Prog. Theor. Phys. **54**, 967 (1975).

[82] A. Yoshimori, Perturbation Analysis on Orbital-Degenerate Anderson Model, Prog. Theor. Phys. **55**, 67 (1976).

[83] C. Mora, P. Vitushinsky, X. Leyronas, A. A. Clerk, and K. Le Hur, Theory of nonequilibrium transport in the $SU(N)$ Kondo regime, Phys. Rev. B **80**, 155322 (2009).

[84] C. Mora, Fermi-liquid theory for $SU(N)$ Kondo model, Phys. Rev. B **80**, 125304 (2009).

[85] C. Mora, C. P. Moca, J. von Delft, and G. Zaránd, Fermi-liquid theory for the single-impurity Anderson model, Phys. Rev. B **92**, 075120 (2015).

[86] M. Filippone, C. P. Moca, A. Weichselbaum, J. von Delft, and C. Mora, At which magnetic field, exactly, does the Kondo resonance begin to split? A Fermi liquid description of the low-energy properties of the Anderson model, Phys. Rev. B **98**, 075404 (2018).

[87] A. Oguri and A. C. Hewson, Higher-Order Fermi-Liquid

Corrections for an Anderson Impurity Away from Half Filling, Phys. Rev. Lett. **120**, 126802 (2018).

[88] A. Oguri and A. C. Hewson, Higher-order Fermi-liquid corrections for an Anderson impurity away from half filling : Equilibrium properties, Phys. Rev. B **97**, 045406 (2018).

[89] A. Oguri and A. C. Hewson, Higher-order Fermi-liquid corrections for an Anderson impurity away from half filling: Nonequilibrium transport, Phys. Rev. B **97**, 035435 (2018).

[90] D. B. Karki, C. Mora, J. von Delft, and M. N. Kiselev, Two-color Fermi-liquid theory for transport through a multilevel Kondo impurity, Phys. Rev. B **97**, 195403 (2018).

[91] D. B. Karki and M. N. Kiselev, Thermoelectric transport through a $SU(N)$ Kondo impurity, Phys. Rev. B **96**, 121403 (2017).

[92] C. P. Moca, C. Mora, I. Weymann, and G. Zaránd, Noise of a Chargeless Fermi Liquid, Phys. Rev. Lett. **120**, 016803 (2018).

[93] C. P. Moca, C. Mora, I. Weymann, and G. Zaránd, Noise of a Chargeless Fermi Liquid, Phys. Rev. Lett. **120**, 016803 (2018).

[94] Y. Teratani, R. Sakano, and A. Oguri, Fermi Liquid Theory for Nonlinear Transport through a Multi-level Anderson Impurity, Phys. Rev. Lett. **125**, 216801 (2020).

[95] A. Oguri, Y. Teratani, K. Tsutsumi, and R. Sakano, Current noise and Keldysh vertex function of an Anderson impurity in the Fermi-liquid regime, Phys. Rev. B **105**, 115409 (2022).

[96] K. Tsutsumi, Y. Teratani, R. Sakano, and A. Oguri, Nonlinear Fermi liquid transport through a quantum dot in asymmetric tunnel junctions, Phys. Rev. B **104**, 235147 (2021).

[97] K. Tsutsumi, Y. Teratani, K. Motoyama, R. Sakano, and A. Oguri, Role of bias and tunneling asymmetries in nonlinear Fermi-liquid transport through an $SU(N)$ quantum dot, Phys. Rev. B **108**, 045109 (2023).

[98] Y. Teratani, K. Tsutsumi, K. Motoyama, R. Sakano, and A. Oguri, Thermoelectric transport and current noise through a multilevel Anderson impurity: Three-body Fermi liquid corrections in quantum dots and magnetic alloys, Phys. Rev. B **110**, 035308 (2024).

[99] K. Motoyama, Y. Teratani, K. Tsutsumi, K. Wake, R. Kobayashi, R. Sakano, and A. Oguri, Three-body Fermi liquid corrections for an infinite- U $SU(N)$ Anderson impurity model, Phys. Rev. B **111**, 235301 (2025).

[100] C. Caroli, R. Combescot, P. Nozieres, and D. Saint-James, Direct calculation of the tunneling current, Journal of Physics C: Solid State Physics **4**, 916 (1971).

[101] L. V. Keldysh, Diagram technique for nonequilibrium processes, Sov. Phys. JETP **20**, 1018 (1965).

[102] H. R. Krishna-murthy, J. W. Wilkins, and K. G. Wilson, Renormalization-group approach to the Anderson model of dilute magnetic alloys. I. Static properties for the symmetric case, Phys. Rev. B **21**, 1003 (1980).

[103] H. R. Krishna-murthy, J. W. Wilkins, and K. G. Wilson, Renormalization-group approach to the Anderson model of dilute magnetic alloys. II. Static properties for the asymmetric case, Phys. Rev. B **21**, 1044 (1980).

[104] A. C. Hewson, A. Oguri, and D. Meyer, Renormalized parameters for impurity models , Eur. Phys. J. B **40**, 177 (2004).

[105] P. Morel and P. Nozières, Lifetime Effects in Condensed Helium-3, Phys. Rev. **126**, 1909 (1962).